

Lepton-flavor violation in light hadron decays

Fajfer, Svjetlana; Ilakovac, Amon

Source / Izvornik: **Physical Review D, Particles and fields, 1998, 57, 4219 - 4235**

Journal article, Published version

Rad u časopisu, Objavljena verzija rada (izdavačev PDF)

<https://doi.org/10.1103/PhysRevD.57.4219>

Permanent link / Trajna poveznica: <https://um.nsk.hr/um:nbn:hr:217:950395>

Rights / Prava: [In copyright](#)/[Zaštićeno autorskim pravom.](#)

Download date / Datum preuzimanja: **2025-01-26**



Repository / Repozitorij:

[Repository of the Faculty of Science - University of Zagreb](#)



Lepton-flavor violation in light hadron decays

S. Fajfer

Institut Jožef Stefan, Jamova 39, P.O. Box 3000, 1001 Ljubljana, Slovenia

A. Ilakovac

University of Zagreb, Faculty of Science, Department of Physics, P.O. Box 162, Bijenička 32, 10000 Zagreb, Croatia

(Received 27 October 1997; published 3 March 1998)

The lepton-flavor-violating decays of light pseudoscalar mesons and light baryons are investigated within extensions of the $SU(2) \times U(1)$ model. These models contain heavy Dirac or Majorana neutrinos and allow large lepton-heavy-neutrino mixings. The free-parameter space of these models is carefully studied. Special care is devoted to the comparison of results of different models. A large “nondecoupling” window is found, and the decoupling of extremely heavy neutrinos is explicitly shown in all models except one, for which the free-parameter space is bounded. Among the decays studied, the experimentally most interesting decays are $K_L \rightarrow e\mu$ and $\pi^0 \rightarrow e\mu$. The $\pi^0 \rightarrow e\mu$ decay is found to be equally interesting for the study of lepton-flavor violation as $K_L \rightarrow e\mu$ decay. The constraint on the model parameters, coming from the nonobservation of the $\mu \rightarrow e\gamma$ decay, leads to the maximal decay rates $B(K_L \rightarrow e\mu) \sim 5 \times 10^{-16}$ and $B(\pi^0 \rightarrow e\mu) \leq (2n_R - 2) \times 10^{-15}$, where n_R is number of heavy neutrinos, much smaller than the present experimental upper limits. [S0556-2821(98)01607-5]

PACS number(s): 13.20.-v, 11.30.Fs, 13.30.Ce, 14.60.St

I. INTRODUCTION

Lepton-flavor violation is strictly forbidden in the standard model (SM). The confirmation of lepton-flavor violation would show that the SM should be considered as a low-energy limit of a more fundamental theory. The slowly decaying particles, such as light pseudoscalar mesons, are suitable to search for lepton-flavor-violating (LFV) effects. Namely, the branching ratios of the LFV decays for such particles are expected to be rather large.

Stringent experimental upper bounds exist for several LFV decays of pseudoscalar mesons, $B(K_L \rightarrow e\mu) < 3.3 \times 10^{-11}$ [1–3], $B(\pi^0 \rightarrow e\mu) < 1.7 \times 10^{-8}$ [1,4], $B(K^+ \rightarrow \pi^+ e\mu) < 2.1 \times 10^{-10}$ [1], and $B(K_L \rightarrow \pi^0 e\mu) < 3.2 \times 10^{-8}$ [5]. The new Brookhaven experiments E871 and E777 should be able to push down the branching ratios $B(\pi^0 \rightarrow e\mu)$ and $B(K^+ \rightarrow \pi^+ e\mu)$ below the $\sim 10^{-12}$ [2]. The measurements of the $B(\pi^0 \rightarrow e\mu)$ is a by-product of measurements of $B(K^+ \rightarrow \pi^+ e\mu)$ [4], and the ratio $B(K^+ \rightarrow \pi^+ e\mu)/B(\pi^0 \rightarrow e\mu)$ is restricted by the acceptance for the decay chain $K^+ \rightarrow \pi^+ \pi^0$, $\pi^0 \rightarrow e\mu$, which is $\sim 10^{-3}$. There is also an upper bound $B(\pi^0 \rightarrow \mu\nu_e) < 1.5 \times 10^{-3}$ [6]. The LFV decays have been the subject of many studies (see, e.g., [6], [7], and [8]). In order to realize the LFV effect a number of approaches have been developed. The simplest one is to add neutral fermions [9,10] or to extend the Higgs sector [11]. They have been also analyzed in supersymmetric models [12], superstring models [13], left-right symmetric models [14,15], technicolor models [16], and leptoquark models [17].

In this paper LFV decays of light pseudoscalar mesons and light baryons are investigated using models with additional heavy neutrinos. LFV decays with two charged leptons in the final state are most likely to be observed. Therefore, we concentrate on analyses of these kinds of decays.

The paper is organized as follows. In Sec. II a short over-

view of the extensions of the standard model with heavy neutrinos is given. In Secs. III, IV, and V the LFV leptonic and semileptonic decay amplitudes of light pseudoscalar mesons and semileptonic decay amplitudes of light baryons, respectively, are analyzed and their branching ratios are calculated. Some technical details are relegated to the Appendixes. The conclusions are given in Sec. V.

II. REMARKS ON MODELS WITH ADDITIONAL HEAVY NEUTRINOS

There are two classes of models which contain the additional heavy neutrinos with light-neutrino masses low enough to satisfy the experimental upper bounds [9,10]. One of them is grand unified theory (GUT) inspired, and it is obtained by introducing an additional n_R right-handed isosinglet neutrino fields into the SM. The Yukawa sector contains lepton-number-conserving ($\Delta L=0$) terms and isosinglet $\Delta L=2$ Majorana mass terms. The neutrino mass matrix is symmetric and consists of a Dirac mass matrix m_D coming from the $\Delta L=0$ Yukawa terms and a Majorana mass matrix m_M containing the $\Delta L=2$ Majorana mass terms. The matrix elements of the Dirac matrix are usually taken to be of the same order as the masses of the charged particles, while the elements of the Majorana mass matrix have much larger values. The transition from the weak to the mass basis gives n_R heavy Majorana neutrinos with masses of the order of a typical Majorana mass and n_G light neutrinos, where n_G is the number of generations in the SM. The experimental limits on light-neutrino masses may be fulfilled in two ways. One is to use the usual seesaw mechanism [18], giving the light-neutrino matrix scaling as $m_D m_M^{-1} m_D$. Then the typical Majorana mass must be very large ($\sim 10^8$ GeV). The second one is realized by imposing an additional constraint on the neutrino mass matrix that assures the masslessness of light neutrinos at the tree level [9]. That can be done if $n_R > 1$. We

will denote such models as An_R . In such models the typical Majorana mass is constrained only by the experimental limits on lepton–heavy-neutrino mixings B_{lN} , which scale as $m_D m_M^{-1}$. The experimental data give the limit $|B_{lN}|^2 \sim 10^{-3} - 10^{-2}$. Therefore, the Majorana masses may be as low as $\sim 10^2$ GeV. The second approach is very appealing from the phenomenological point of view. Namely, the B_{lN} mixings lead to decays which are forbidden in the SM. In the model [9], B_{lN} mixings may be so large that the rates of these decays could be comparable in size to the present experimental upper bounds. Although the masses of light neutrinos are zero at the tree level, nonzero masses may be induced radiatively [19]. They depend on the choice of the renormalization point, and may be quite large compared with the experimental and astrophysical upper limits on light neutrino masses. The second class of models is stable regarding the neutrino mass renormalization and renormalization of B_{lN} mixings [19], and, therefore, we prefer the results obtained in these models.

The second class of models is superstring inspired [10,21,22]. These models, referred to here as Vn_R models, are obtained by introducing n_R isosinglet right-handed and n_R isosinglet left-handed neutrino fields into the SM, which do not interact with SM fields. The Yukawa sector contains only the lepton-number-conserving terms. The neutrino mass matrix \mathcal{M}^ν [22,23] is symmetric and contains a matrix m_D , coupling the doublet neutrinos with right-handed singlet neutrinos, and a matrix M , coupling the right-handed and left-handed singlet neutrinos. The rank of the mass matrix is $2n_R$. Therefore, it has n_G zero eigenvalues. As the neutrino mass matrix is symmetric, the mass diagonalization can be performed by unitary transformations of the form $U^T \mathcal{M}^\nu U$. The diagonalization is performed in two steps [23]. First, the elements of the mass submatrix m_D are cancelled, using the unitary transformation of the mentioned form. The n_G doublet neutrino fields and n_R singlet left-handed neutrino fields are combined into n_G massless neutrino fields and n_R fields forming the mass matrix M_D with the right-handed singlet fields. Then another unitary transformation is used to diagonalize the mass matrix M_D . The final mass spectrum contains n_G exactly massless (to all orders in perturbation theory) left-handed neutrinos (that is, the Weyl neutrinos) and n_R massive Dirac neutrinos. The massless and massive neutrino fields contain part of the weak eigenstate doublet fields, and, therefore, both interact with SM fields, specifically leptons, gauge bosons, and Higgs scalars. The corresponding Lagrangians defining the interaction vertices are (see Refs. [20,24])

$$\mathcal{L}_{int}^W = -\frac{g_W}{2\sqrt{2}} W^{-\mu} \sum_{i=1}^{n_G} \sum_{j=1}^{n_G+n_R} B_{l_i n_j} \bar{l}_i \gamma_\mu (1 - \gamma_5) n_j + \text{H.c.}, \quad (1)$$

$$\mathcal{L}_{int}^Z = -\frac{g_W}{4c_W} Z^\mu \sum_{i,j=1}^{n_G+n_R} C_{n_i n_j} \bar{n}_i \gamma_\mu (1 - \gamma_5) n_j, \quad (2)$$

$$\mathcal{L}_{int}^{G^\pm} = -\frac{g_W}{2\sqrt{2}M_W} G^\pm \sum_{i=1}^{n_G} \sum_{j=1}^{n_G+n_R} B_{l_i n_j} \bar{l}_i [m_{l_i} (1 - \gamma_5) - m_{n_j} (1 + \gamma_5)] n_j + \text{H.c.}, \quad (3)$$

$$\mathcal{L}_{int}^{G^0} = \frac{ig_W}{4M_W} G^0 \sum_{i,j=1}^{n_G+n_R} C_{n_i n_j} m_{n_j} \bar{n}_i (1 + \gamma_5) n_j, \quad (4)$$

$$\mathcal{L}_{int}^H = -\frac{g_W}{4M_W} H \sum_{i,j=1}^{n_G+n_R} C_{n_i n_j} m_{n_j} \bar{n}_i (1 + \gamma_5) n_j, \quad (5)$$

where l_i are the SM leptons, n_i are the (light and heavy) neutrino fields, Z and W^\pm are the SM gauge bosons, H is the Higgs scalar field, and G^\pm and G^0 are unphysical Goldstone bosons. Further, g_W is the weak coupling constant, $c_W = M_W^2/M_Z^2$, and m_i , $i=1, \dots, n_G+n_R$ are neutrino masses. As in the case of the first class of models, a Cabibbo–Kobayashi–Maskawa type of matrix B_{ln} appears in lepton–neutrino–charged currents and mixing matrices $C_{nn'}$ in neutral neutrino currents. These matrices are composed of unitary matrices transforming leptons and neutrinos from the weak to the mass basis. The matrix $C_{nn'}$ may be expressed in terms of B_{ln} matrices. The B and C matrices satisfy a set of relations following from the unitarity of the matrices building them [9,19,20,25]:

$$\begin{aligned} \sum_{k=1}^{n_G+n_R} B_{l_1 n_k} B_{l_2 n_k}^* &= \delta_{l_1 l_2}, & \sum_{k=1}^{n_G+n_R} C_{n_i n_k} C_{n_j n_k}^* &= C_{n_i n_j}, \\ \sum_{k=1}^{n_G+n_R} B_{l n_k} C_{n_k n_i} &= B_{l n_i}, & \sum_{k=1}^{n_G} B_{l n_i}^* B_{l n_j} &= C_{n_i n_j}, \end{aligned} \quad (6)$$

which assure the renormalizability of the models. In the first class of models, the B matrices satisfy the same set of relations, and in addition they are constrained by relations which assure the masslessness of the light neutrinos at the tree level.

The degeneracy of light neutrinos in Vn_R models allows one to write the light-neutrino–lepton–charged currents in an almost diagonal form, with couplings somewhat smaller than in SM:

$$g_{W \rightarrow} \rightarrow g_W \times B_{l\nu_l}. \quad (7)$$

This small reduction of couplings is connected with couplings in heavy-neutrino–lepton–charged currents B_{lN} , through the orthogonality relations which the B_{ln} matrices satisfy,

$$|B_{l\nu_l}|^2 \approx \sum_{i=1}^{n_G} |B_{l\nu_i}|^2 = (c_L^{\nu_l})^2 = 1 - \sum_{i=1}^{n_R} |B_{lN_i}|^2 = 1 - (s_L^{\nu_l})^2. \quad (8)$$

The experimental upper limits [15,28]

$$(s_L^{v_e})^2 < 0.0071,$$

$$(s_L^{v_\mu})^2 < 0.0014$$

$$(s_L^{v_\tau})^2 < 0.01,$$

$$(s_L^{v_e})^2 (s_L^{v_\mu})^2 < 5.6 \times 10^{-8} \quad (9)$$

assure that the deviation of the light-neutrino–lepton mixings from the SM mixings is small, and that the heavy-neutrino–lepton mixings $|B_{lN_i}|^2$ are of the order $\lesssim 10^{-3} - 10^{-2}$.

Using relations (6), all amplitudes of low-energy processes may be written in terms of

$$\sum_{i=1}^{n_R} B_{lN_i}^* B_{l'N_i} f(N_i, \dots), \quad \sum_{j=1}^{n_G} V_{u_j d_a} V_{u_j d_a}^* f(u_j, \dots),$$

$$\text{and } \sum_{j=1}^{n_G} V_{ud_j} V_{ud_j}^* f(d_j, \dots), \quad (10)$$

where $f(N_i, \dots)$, $f(u_j, \dots)$, and $f(d_j, \dots)$ are expressions proportional to loop functions. The ellipses represent the indices not written explicitly. In the first type of models, the B and C matrices satisfy additional constraints besides those given by Eqs. (6). These constraints reduce the number of free parameters determining the B and C matrices. For $n_R = 2$, the B and C matrices are completely determined. Therefore, the first of expressions (10) may be calculated exactly. For $n_R > 2$, the number of constraints on the B and C matrices is too small to fix them. In the second class of models, the B and C matrices satisfy only relations (6), and their exact form cannot be determined, too. Only the upper bounds on the absolute values of matrix elements B_{lN} may be found. The upper limits of the branching ratios can be obtained using the Schwartz's inequalities and definition for $s_L^{v_l}$,

$$\left| \sum_{i=1}^{n_R} B_{lN_i}^* B_{l'N_i} f(N_i, \dots) \right| \leq s_L^{v_l} s_L^{v_{l'}} \left(\langle |f(\dots)| \rangle_N + \left[\sum_{i=1}^{n_R} \langle f(N_i, \dots) \rangle_N^2 \right]^{1/2} \right),$$

$$\left| \sum_{j=1}^{n_R} V_{u_j d_a} V_{u_j d_a}^* f(u_j, \dots) \right| \leq \sum_{j=1}^{n_R} |V_{u_j d_a}| |V_{u_j d_a}| |f(u_j, \dots)|,$$

$$\left| \sum_{j=1}^{n_R} V_{ud_j} V_{ud_j}^* f(d_j, \dots) \right| \leq \sum_{j=1}^{n_R} |V_{ud_j}| |V_{ud_j}| |f(d_j, \dots)|, \quad (11)$$

where $\langle \rangle_N$ represents an average over heavy neutrinos. The procedure for deriving relations (11) is given in Appendix B, and is used for finding the upper limits on composite loop form factors and branching ratios.

Although there are no constraints on heavy-neutrino masses from experimental limits on light-neutrino masses, they are limited by perturbative unitarity condition [29] on decay rates of heavy neutrinos,

$$\frac{\Gamma_{N_i}}{m_{N_i}} < \frac{1}{2}. \quad (12)$$

The total decay rate of the heavy Dirac neutrino of a mass m_{N_i} much larger than masses of W and Z bosons and Higgs boson mass is [20]

$$\Gamma_{N_i} = \sum_{l_j} \Gamma(N_i \rightarrow l_j^- W^+) + \sum_{\nu_j} [\Gamma(N_i \rightarrow \nu_j Z) + \Gamma(N_i \rightarrow \nu_j H)]$$

$$\approx \frac{\alpha_W}{8M_W} m_{N_i}^3 \sum_j |B_{l_j N_i}|^2, \quad (13)$$

where $\alpha_W = g^2/4\pi$. From Eqs. (12) and (13),

$$m_{N_i}^2 \sum_{j=1}^{n_G} |B_{l_j N_i}|^2 = m_{N_i}^2 C_{N_i N_i} \leq \frac{4}{\alpha_W} M_W^2, \quad (14)$$

for Vn_R models, and

$$m_{N_i}^2 \sum_{j=1}^{n_G} |B_{l_j N_i}|^2 = m_{N_i}^2 C_{N_i N_i} \leq \frac{2}{\alpha_W} M_W^2, \quad (15)$$

for An_R models. The relative factor of 2 between the bounds (14) and (15) comes from the different number of spin degrees of freedom of Dirac and Majorana neutrinos. The matrix elements $C_{N_i N_i}$ are known only in the $A2$ model, which makes a large difference between that model and the other models discussed here. In the $A2$ model, the matrix elements $C_{N_i N_i}$ depend on the ratio of masses $\rho_2 = m_{N_2}/m_{N_1}$, and not on the masses explicitly, so that both parts of Eq. (15) are upper bounds on the lightest mass m_{N_1} . Equation (15) for the m_{N_2} mass gives stronger bound on m_{N_1} ;

$$m_{N_1}^2 \leq \frac{2M_W^2}{\alpha_W} \frac{\rho_2^{-1} + \rho_2^{-2}}{\sum_{j=1}^{n_G} (s_l^{v_j})^2}. \quad (16)$$

In An_R , $n_R \neq 2$, models and in Vn_R models, the upper bound on the lightest mass is obtained by combining Eqs. (14) and (8),

$$m_{N_1}^2 \leq (m_{N_1}^0)^2 \left(1 + \sum_{i=2}^{n_R} \rho_i^{-2} \right), \quad (17)$$

where $\rho_i = m_{N_i}/m_{N_1}$ and

$$(m_{N_1}^0)^2 = 4bM_W^2 / [\alpha_W \sum_{j=1}^{n_G} (s_l^{v_j})^2],$$

with $b = 1$ in Vn_R models and $b = 1/2$ in An_R , $n_R \neq 2$, models. Equation (16) permits only finite values of all heavy-neutrino masses, while the masses m_{N_i} , $i \neq 1$ satisfying Eq. (17) may achieve any value if $m_{N_1} < m_{N_1}^0$. If Eqs. (11) were

used for evaluating the upper bounds on the branching ratios (UBBRs) for LFV processes, the UBBRs would achieve infinite values. Therefore, if $m_{N_1} < m_{N_1}^0$ and any of the ratios ρ_i is very large, the UBBRs have to be evaluated in a different manner. Noticing that Eqs. (8) and (14) give rough upper bounds,

$$|B_{IN_i}| \leq s_L^{v_i} \equiv B_{IN_i}^1 \quad (18)$$

and

$$|B_{IN_i}| \leq \frac{2b^{1/2}M_W}{\alpha_W^{1/2}m_{N_i}} \equiv B_{IN_i}^0, \quad (19)$$

one finds that if

$$B_{IN_i}^0 < B_{IN_i}^1 \quad (20)$$

for any matrix element B_{IN_i} , the better bound on the UBBRs of LFV processes may be achieved by replacing the matrix elements B_{IN_i} by $B_{IN_i}^0$ in the amplitudes. With such a replacement, the terms of the amplitudes comprising the mass m_{N_i} do not tend to infinity but to zero in the $m_{N_i} \rightarrow \infty$ limit. That is, the heavy neutrino decouples from the light sector of the model. As the A2 model is a special case of An_R models, the decoupling of the extremely heavy neutrinos is valid for it, too. That property cannot be seen in the A2 model because the domain of m_{N_i} masses is restricted by Eq. (16).

III. MESON LFV LEPTONIC DECAYS

The amplitudes of LFV leptonic decays of kaons into two charged leptons have a very simple structure. Only a box diagram contributes to them. These box diagrams have a very mild (logarithmic) dependence on the heavy-neutrino masses [26,27]. They are suppressed by matrix elements of Cabibbo-Kobayashi-Maskawa (CKM) matrix elements in the hadronic part of the matrix element. The corresponding decay rates for flavor-neutral pseudoscalar mesons is not CKM suppressed, and the matrix element has an additional Z-boson exchange contribution with a strong (quadratic) dependence on the heavy-neutrino mass (the vector mesons have an additional γ -decay channel). Unfortunately, flavor-neutral pseudoscalar mesons decay at least 10^6 times faster than the mesons with nonzero quantum numbers due to the electromagnetic and hadronic channels through which they decay. To determine to what extent these two opposite effects, concerning the magnitude of the decay rate, cancel, the decay rates for the processes $\pi^0 \rightarrow e\mu$ and $\eta^0 \rightarrow e\mu$ have been evaluated, too. The decay $\eta'^0 \rightarrow e\mu$ has not been considered as η' decays much faster than π^0 and η .

The invariant amplitude $T(P^0 \rightarrow e^- \mu^+)$ and the decay rate $\Gamma(P^0 \rightarrow e^- \mu^+)$ or branching ratio $B(P^0 \rightarrow e^- \mu^+)$ for the decay of a light pseudoscalar meson into an electron and antimuon, $P^0 \rightarrow e^- \mu^+$, may be obtained from the corresponding expressions for $\tau^- \rightarrow e^- P^0$ decays [26] using the crossing symmetry. The expression for the invariant amplitude is

$$T(P^0 \rightarrow e^- \mu^+) = -\bar{u}_e \gamma_\alpha (1 - \gamma_5) v_\mu p_{P^0}^\alpha a_{\bar{P}^0}^{\mu e}, \quad (21)$$

where p_{P^0} is the four-momentum of the pseudoscalar meson and \bar{P}^0 is its antiparticle. The composite form factor $a_{\bar{P}^0}^{\mu e}$ is given by

$$a_{\bar{P}^0}^{\mu e} = \frac{i\alpha_W^2}{16M_W^2} f_{P^0} \left[\alpha_Z F_Z^{\mu e} + \alpha_{box}^{uu} F_{box}^{\mu e uu} + \sum_{d_a, d_b = d, s} \alpha_{box}^{d_a d_b} F_{box}^{\mu e d_a d_b} \right], \quad (22)$$

where $\alpha_W = g_W^2/4\pi$, f_{P^0} is a pseudoscalar decay constant, $F_Z^{\mu e}$, $F_{box}^{\mu e uu}$, $F_{box}^{\mu e d_a d_b}$ are composite loop form factors defined in Appendix A and in Refs. [26,27], and $\alpha_{box}^{ds}(K^0) = 2^{1/2}$, $\alpha_{box}^{sd}(\bar{K}^0) = 2^{1/2}$, $\alpha_Z(\pi^0) = -2$, $\alpha_{box}^{uu}(\pi^0) = -1$, $\alpha_{box}^{dd}(\pi^0) = -1$, $\alpha_Z(\eta^0) = -\alpha_{box}^{ss}(\eta^0) = -(2c_P/3^{1/2} + (2/3)^{1/2}s_P)$, $\alpha_{box}^{uu}(\eta^0) = -\alpha_{box}^{dd}(\eta^0) = -(c_P/3^{1/2} - (2/3)^{1/2}s_P)$

are numerical coefficients containing information about the quark content of pseudoscalars and on quark couplings with photons and Z bosons (only coefficients different from zero are listed). The shorthand notation $s_P = \sin\theta_P$ and $c_P = \cos\theta_P$ is used for mixing of octet and singlet meson states. The pseudoscalar decay constants (and the normalization of creation operators) are defined in terms of the axial vector quark currents,

$$A_\mu^{P^0}(x) = i\sqrt{2}f_{P^0}\partial_\mu P^0(x) + \dots \quad (23)$$

The composite loop form factors $F_Z^{\mu e}$, $F_{box}^{\mu e uu}$, and $F_{box}^{\mu e d_a d_b}$ comprise the combinations of C_{NN} and B_{IN} matrix elements, which are all proportional to a factor smaller than $s_L^{v_e} s_L^{v_\mu}$. That factor strongly suppresses the $T(P^0 \rightarrow e^- \mu^+)$ amplitudes. The branching ratio corresponding to the amplitude (21) reads

$$B(P^0 \rightarrow e^- \mu^+) = \frac{1}{4\pi} \frac{m_{P^0}}{\Gamma_{P^0}} \frac{\lambda^{1/2}(m_{P^0}^2, m_\mu^2, m_e^2)}{m_{P^0}^2} \times |a_{\bar{P}^0}^{\mu e}|^2 \frac{m_{P^0}^2(m_\mu^2 + m_e^2) - (m_\mu^2 - m_e^2)^2}{m_{P^0}^2}, \quad (24)$$

where m_{P^0} and Γ_{P^0} are the pseudoscalar meson mass and total decay rate, and $\lambda(x, y, z) = x^2 + y^2 + z^2 - 2(xy + xz + yz)$.

IV. MESON LFV SEMILEPTONIC DECAYS

In the case of LFV $K^+ \rightarrow \pi^+ e^- \mu^+$ decay on the quark-lepton level there are contributions coming from a box diagram and W^+W^- diagram. The W^+W^- contribution is found to be much smaller than the box diagram contribution [27], and, therefore, it will be neglected. The box amplitude may be obtained from the box amplitude for the $\tau^- \rightarrow e^- \pi^+ K^-$ decay using crossing symmetry and replacing τ by μ . It reads

$$\begin{aligned}
T_{box}(K^+ \rightarrow \pi^+ e^- \mu^+) &= -a_{K^+ \pi^+}^{\mu e} \bar{u}_e \gamma_\alpha (1 - \gamma_5) v_\mu \\
&\times \langle \pi^+(p_{\pi^+}) | \bar{s}(0) \gamma^\mu (1 - \gamma_5) \\
&\times d(0) | K^+(p_{K^+}) \rangle, \quad (25)
\end{aligned}$$

where

$$a_{K^+ \pi^+}^{\mu e} = \frac{i \alpha_W^2}{16 M_W^2} F_{box}^{\mu esd} \quad (26)$$

is a composite form factor comprising a factor of order $\sim s_L^\nu e s_L^\nu$. The hadronic matrix element for $K^+ \rightarrow \pi^+ e^- \mu^+$ decay is parametrized by two form factors

$$\begin{aligned}
\langle \pi^+(p_{\pi^+}) | \bar{s}(0) \gamma^\mu (1 - \gamma_5) d(0) | K^+(p_{K^+}) \rangle \\
= f_+(q^2) (p_{K^+} + p_{\pi^+})^\mu + f_-(q^2) (p_{K^+} - p_{\pi^+})^\mu. \quad (27)
\end{aligned}$$

In this paper we use a chiral Lagrangian which includes vector mesons [30] in order to evaluate this matrix element. This approach assumes that the vector meson exchange dominates the form factors. The quark legs of the box diagram (\bar{s} and d fields) create the vector meson field K^{0*} , which further couples to the pion and kaon fields. The coupling of the K^{0*} field to the quark fields (K^{0*} meson decay constant, $m_{K^{0*}}^2 / \sqrt{2} \gamma_{K^{0*}}$) is related to the coupling of ρ^0 mesons ($m_{\rho^0}^2 / \sqrt{2} \gamma_{\rho^0}$), assuming $SU(3)$ hadron flavor symmetry ($\gamma_{K^{0*}} = \gamma_{\rho^0}$). The ρ -meson coupling is determined from the $\rho^0 \rightarrow e^+ e^-$ decay rate. The vector meson to pseudoscalar meson coupling $g_{\rho\pi\pi}$ is defined in the chiral Lagrangian [30] and it can be calculated from the $\rho \rightarrow \pi\pi$ decay rate. The hadronic part of the amplitude reads

$$\begin{aligned}
\langle \pi^+(p_{\pi^+}) | \bar{s}(0) \gamma_\mu (1 - \gamma_5) d(0) | K^+(p_{K^+}) \rangle \\
= \frac{m_{K^{0*}}^2}{\sqrt{2} \gamma_{K^{0*}}} i S_{K^{0*}, \mu\nu}(q) T^\nu(K^+; K^{0*} \pi^+), \\
\approx \frac{g_{\rho\pi\pi}}{2 \gamma_{K^{0*}}} \left[\left(1 + \frac{m_{\pi^+}^2}{m_{K^{0*}}^2} \frac{q^2}{m_{\pi^+}^2} \right) (p_{K^+} + p_{\pi^+})_\mu \right. \\
\left. + \left(-\frac{m_{\pi^+}^2}{m_{K^{0*}}^2} \frac{m_{K^+}^2 - m_{\pi^+}^2}{m_{\pi^+}^2} \right) (p_{K^+} - p_{\pi^+})_\mu \right], \quad (28)
\end{aligned}$$

where

$$S_{K^{0*}}^{\alpha\beta}(q) = \frac{-g^{\alpha\beta} + q^\alpha q^\beta / m_{K^{0*}}^2}{q^2 - m_{K^{0*}}^2} \quad (29)$$

is the K^{0*} -meson propagator, and

$$T^\nu(K^+; K^{0*} \pi^+) = \frac{-i g_{\rho\pi\pi}}{\sqrt{2}} (p_{K^+} + p_{\pi^+})^\nu \quad (30)$$

is the $K^+ - K^{0*} - \pi^+$ vertex. The details of evaluation of the hadronic part of the amplitude may be found in [27], where

they have been performed for $\tau \rightarrow e +$ two meson decays. This method assumes $SU(3)$ hadron-flavor symmetry, and, therefore, it connects the amplitudes of various mesons, specifically of decays $K^0 \rightarrow \pi^0 e^- \mu^+$ and $\bar{K}^0 \rightarrow \pi^0 e^- \mu^+$, allowing one to evaluate the $K_L \rightarrow \pi^0 e^- \mu^+$ amplitude. Namely, we determine

$$f_+(0) = \frac{g_{\rho\pi\pi}}{2 \gamma_{K^{0*}}} \approx 1.2,$$

$$f_+(q^2) \approx f_+(0) \left(1 + \frac{m_{\pi^+}^2}{m_{K^{0*}}^2} \frac{q^2}{m_{\pi^+}^2} \right),$$

$$f_-(q^2) \approx f_+(0) \left(-\frac{m_{\pi^+}^2}{m_{K^{0*}}^2} \frac{m_{K^+}^2 - m_{\pi^+}^2}{m_{\pi^+}^2} \right). \quad (31)$$

From the semileptonic decays K_{e3}^+ and $K_{\mu 3}^+$ the hadronic matrix element is

$$\begin{aligned}
\langle \pi^0(p_{\pi^0}) | \bar{s}(0) \gamma^\mu (1 - \gamma_5) u(0) | K^+(p_{K^+}) \rangle \\
= \frac{1}{\sqrt{2}} [f_+(q^2) (p_{K^+} + p_{\pi^+})^\mu \\
+ f_-(q^2) (p_{K^+} - p_{\pi^+})^\mu], \quad (32)
\end{aligned}$$

and the form factors are described by [31]

$$f_\pm(q^2) = f_+(0) \left[1 + \lambda_\pm \frac{q^2}{m_\pi^2} \right], \quad (33)$$

where $\lambda_+ = 0.0286 \pm 0.0022$ for K_{e3}^+ and $\lambda_+ = 0.033 \pm 0.008$ for $K_{\mu 3}^+$. Usually, instead of the form factor f_- , the scalar form factor is introduced,

$$f_0(q^2) = f_+(q^2) + \frac{q^2}{M_K^2 - M_\pi^2} f_-(q^2) = f_+(0) \left[1 + \lambda_0 \frac{q^2}{m_\pi^2} \right], \quad (34)$$

with $\lambda_0 = 0.004 \pm 0.007$ and $f_+(0) = 0.98$. Using isospin symmetry, $\langle \pi^+ | \bar{s} \gamma^\mu (1 - \gamma_5) d | K^+ \rangle$ can be related to the $\langle \pi^0 | \bar{s} \gamma^\mu (1 - \gamma_5) u | K^+ \rangle$ matrix element. Our results in Eqs. (31) [$\lambda_+ = m_{\pi^+}^2 / m_{K^{0*}}^2 = 0.024$, $\lambda_0 = 0$, $f_+(0) \approx 1.2$] are in agreement with these phenomenological results up to $SU(3)$ hadron flavor symmetry violation.

The $K_L^0 \rightarrow \pi^0 e^- \mu^+$ and $\eta \rightarrow \pi^0 e^- \mu^+$ have vanishing amplitudes, as can be seen from the chiral Lagrangian (see Appendix C). The first decay can occur through the CP -violating component, but the induced decay rate is very suppressed in comparison with $K^+ \rightarrow \pi^+ e^- \mu^+$.

The branching ratio for the remaining $K^+ \rightarrow \pi^+ e^- \mu^+$ decay is found to be

$$\begin{aligned}
& B(K^+ \rightarrow \pi^+ e^- \mu^+) \\
&= \frac{1}{64\pi^3 m_{K^+}^3 \Gamma_{K^+}} |a_{K^+ \pi^+}^{\mu e}|^2 \int \frac{(m_{K^+} - m_{\pi^+})^2}{(m_{\mu^+} + m_e)^2} dt [A_{++} f_+^2 \\
&\quad + A_{+-} f_+ f_- + A_{--} f_-^2], \tag{35}
\end{aligned}$$

where A_{++} , A_{+-} , and A_{--} are kinematical functions defined in Appendix D.

V. BARYON LFV SEMILEPTONIC DECAYS

In the LFV baryon decays with two charged leptons, due to kinematical reasons, the final and initial baryon states do not have the same strangeness. Therefore, on the quark-lepton level, the decay amplitudes obtain contributions from the box diagram only.

The matrix element for the baryonic LFV semileptonic decay is obtained from mesonic semileptonic decay matrix elements by replacing the hadronic meson-to-meson amplitude by the baryon-to-baryon amplitude. The baryon-to-baryon amplitude depends on six form factors

$$\begin{aligned}
\langle B' | V_\mu(0) - A_\mu(0) | B \rangle &= \bar{u}_{B'} [\gamma_\mu f_1 + i \sigma_{\mu\nu} q^\nu f_2 + q_\mu f_3 \\
&\quad + \gamma_\mu \gamma_5 g_1 + i \sigma_{\mu\nu} \gamma_5 q^\nu g_2 \\
&\quad + q_\mu \gamma_5 g_3] u_B. \tag{36}
\end{aligned}$$

However, all of them are not equally important. The currents whose coefficients are f_3 and g_2 do not conserve G parity (second class currents). Therefore, these form factors are negligibly small. The f_2 term includes the recoil effects, and is of the order of $(m_B - m_{B'})/(m_B + m_{B'})$ compared to the f_1 term. Since we are making an estimation of the branching ratios, we do not take into account these terms. The g_3 term contains a pseudoscalar meson pole, and its contribution is not negligible when the muon is in the final state [31].

The form factors f_1 , g_1 , and g_3 depend on baryons in the initial and final states. Further, the q^2 dependence may be approximately described by assigning a pole dependence of the meson having the same Lorentz transformation properties and opposite quantum numbers than the baryon current. The $SU(3)$ -flavor symmetry of baryons allows one to express sets of f_1 , g_1 , and g_3 form factors in terms of $SU(3)$ Clebsch-Gordan coefficients and two functions per set, one corresponding to the symmetric octet representation and the other to the antisymmetric one. Because of the isospin invariance, the symmetric octet cannot contribute to the vector current form factors. Next, the pairs of the functions describing g_1 and g_3 form factors are not independent, but correlated through the Goldberger-Treiman relation. The Goldberger-Treiman relation extrapolates the baryon-baryon-meson ($g_{BB'M}$) strong coupling constant at $q^2 = m_M^2$ to its $q^2 = 0$ value. The pole dominance of the g_3 form factor of the $\Delta S = 1$ hadronic matrix elements is carried by kaons, and, therefore, this extrapolation may lead to a $\sim 10\%$ error in g_3 values — good enough for our purposes (in Ref. [32] the semileptonic LFV baryon decays were evaluated including the f_2 form factor in calculations). After applying all of the above-mentioned approximations, the final form of the hadronic matrix elements reads

TABLE I. The values of the form factors f_1 and g_1 at zero momentum transfer.

Process	$f_1(0)$	$g_1(0)$
$\Sigma^+ \rightarrow p e^- \mu^+$	-1	$-D + F$
$\Sigma^0 \rightarrow n e^- \mu^+$	$-\frac{1}{\sqrt{2}}$	$-\frac{D}{\sqrt{2}} + \frac{F}{\sqrt{2}}$
$\Lambda \rightarrow n e^- \mu^+$	$-\frac{3}{\sqrt{6}}$	$\frac{D}{\sqrt{6}} + \frac{3F}{\sqrt{6}}$
$\Xi^0 \rightarrow \Lambda e^- \mu^+$	$\frac{3}{\sqrt{6}}$	$-\frac{D}{\sqrt{6}} + \frac{3F}{\sqrt{6}}$
$\Xi^0 \rightarrow \Sigma^0 e^- \mu^+$	$-\frac{1}{\sqrt{2}}$	$-\frac{D}{\sqrt{2}} + \frac{F}{\sqrt{2}}$
$\Xi^- \rightarrow \Sigma^- e^- \mu^+$	1	$-D - F$

$$\begin{aligned}
\langle B' | V_\mu(0) - A_\mu(0) | B \rangle &\approx \bar{u}_{B'} [\gamma_\mu f_1^{B'B} + \gamma_\mu \gamma_5 g_1^{B'B} \\
&\quad + q_\mu \gamma_5 g_3^{B'B}] u_B \\
&\approx \bar{u}_{B'} \left[f_1^{B'B}(0) \gamma_\mu + g_1^{B'B}(0) \right. \\
&\quad \left. \times \left(\gamma_\mu \gamma_5 + q_\mu \gamma_5 \frac{m_B + m_{B'}}{m_{K^0} - q^2} \right) \right] u_B, \tag{37}
\end{aligned}$$

where $f_1(0)$ and $g_1(0)$ are given in Table I.

The vector and axial-vector form factors have a very weak q^2 dependence, determined by the vector and axial-vector meson poles and, therefore, in the following, we consider them as constants. Since the largest momentum transfer for all decays of our interest, $(m_{\Sigma^+} - m_p)^2$, is much smaller than any of the vector meson or axial-vector meson masses, the q^2 dependence of these two form factors may also be neglected.

Hence, the expression for the $B \rightarrow B' e^- \mu^+$ amplitudes is given by

$$\begin{aligned}
T(B \rightarrow B' e^- \mu^+) &= a_{BB'}^{\mu e} \bar{u}_e \gamma_\alpha (1 - \gamma_5) v_\mu \bar{u}_{B'} \\
&\quad \times \left[f_1^{BB'}(0) \gamma_\alpha + g_1^{BB'}(0) \right. \\
&\quad \left. \times \left(\gamma_\mu \gamma_5 + q_\mu \gamma_5 \frac{m_B + m_{B'}}{m_{K^0} - q^2} \right) \right] u_B, \tag{38}
\end{aligned}$$

where again the composite form factor

$$a_{BB'}^{\mu e} = \frac{i \alpha_W^2}{16 M_W^2} F_{box}^{\mu eds} \tag{39}$$

contains a factor of the order of $s_L^{\nu e} s_L^{\nu \mu}$. The branching ratio $B(B \rightarrow B' e^- \mu^+)$ is given by

$$\begin{aligned}
B(B \rightarrow B' e^- \mu^+) &= \frac{1}{4\pi^3 m_B^3 \Gamma_B} |a_{BB'}^{\mu e}|^2 \int_{(m_\mu + m_e)^2}^{(m_B - m_{B'})^2} dt \\
&\times [A_1(f_1^2 + g_1^2) + A_2(f_1^2 - g_1^2) + A_3(f_1 g_1) \\
&+ A_4(g_1 g_3) + A_5(g_3^2)]. \quad (40)
\end{aligned}$$

$A_1 - A_5$ are kinematical functions defined in Appendix D.

VI. NUMERICAL RESULTS

The numerical analysis of the results is performed for the extensions of the SM with two or more heavy neutrinos. The $n_R=2$ case is treated with the special care since it allows a comparison with the $n_R=2$ version of the theory with heavy Majorana neutrinos for which the B and C matrices may be evaluated exactly. The additional parameters of the model(s) introduced with heavy neutrinos are three heavy-neutrino-lepton mixings $s_L^{\nu l}$ and heavy-neutrino masses m_{N_i} . The $s_L^{\nu l}$ are constrained by experimental upper limits (10), while the upper limit on the heavy-neutrino masses is given by perturbative-unitarity relations (14) and (15). For upper limit of $(s_L^{\nu \mu})^2$ we take the ratio of upper limits of $(s_L^{\nu e})^2 (s_L^{\nu \mu})^2$ and $(s_L^{\nu e})^2$.

The numerical results depend also on hadronic observables and quark parameters. In the calculations, the experimental (absolute) values for the CKM-matrix elements are used [1] and the quark-mass values [1,33,34]

$$\begin{aligned}
m_u &= 0.005 \text{ GeV}, & m_d &= 0.010 \text{ GeV}, \\
m_s &= 0.199 \text{ GeV}, & m_c &= 1.35 \text{ GeV}, \\
m_b &= 4.3 \text{ GeV}, & m_t &= 176 \text{ GeV}. \quad (41)
\end{aligned}$$

For the pseudoscalar decay constants, experimental values are used [1],

$$f_{\pi^0} = 84.1 \text{ MeV}, \quad f_{K^\pm} = 113 \text{ MeV}, \quad f_\eta = 94 \text{ MeV}, \quad (42)$$

and due to isospin symmetry, $f_{K^0} = f_{\bar{K}^0} \approx f_{K^\pm}$.

With the input parameters defined above, one can start a discussion of the numerical results. We are interested in the branching ratios of LFV leptonic and semileptonic decays of light pseudoscalar mesons and LFV semileptonic decays of light baryons. Numerical results are presented only for the most interesting decays, that is, for decays of particles with small total decay widths and/or strong LFV decay channels:

$$\begin{aligned}
&K_L \rightarrow e\mu, \quad \pi^0 \rightarrow e\mu, \quad \eta \rightarrow e\mu, \\
&K^+ \rightarrow \pi^+ e\mu, \\
&\Sigma^+ \rightarrow p e\mu, \quad \Sigma^0 \rightarrow n e\mu, \quad \Lambda \rightarrow p e\mu, \\
&\text{and } \Xi^0 \rightarrow \Lambda e\mu. \quad (43)
\end{aligned}$$

For instance, $\eta' \rightarrow e\mu$ is not studied because η' has a large total decay width compared to other flavor-neutral pseudoscalar mesons. Similarly, the $\Xi^0 \rightarrow \Sigma^0 e^- \mu^+$ and Ξ^-

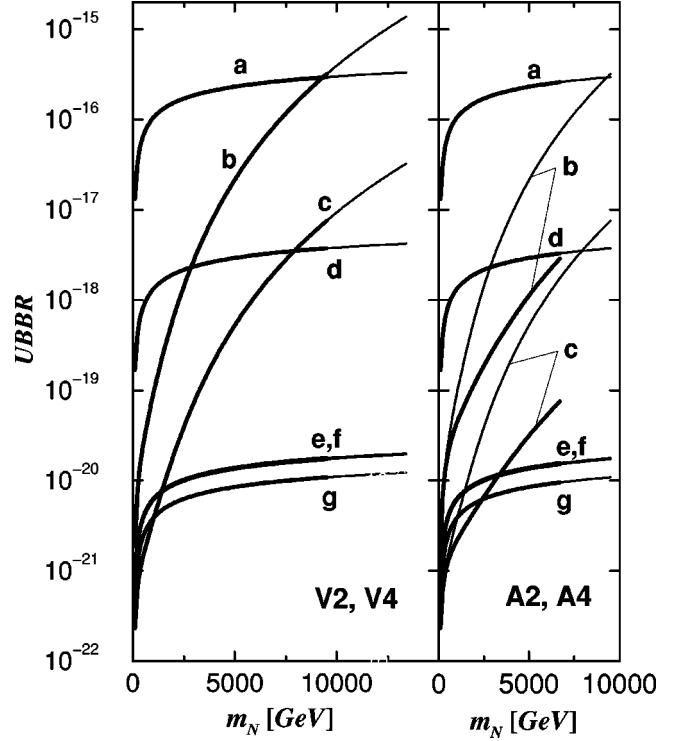


FIG. 1. The UBBRs for the most interesting LFV hadron decays versus $m_N = m_{N_i}$, $i=1, n_R$ in models V2, V4, A2, and A4.

$\rightarrow \Sigma^- e^- \mu^+$ decays are not discussed since they are strongly phase-space suppressed compared to other LFV baryon decays.

The numerical results are shown in five figures and in one table. If $(s_L^{\nu l})^2$ values are not explicitly stated, the results in the figures are evaluated for maximal $(s_L^{\nu l})^2$ mixings, $(s_L^{\nu e})^2 = 0.0071$, $(s_L^{\nu e})^2 (s_L^{\nu \mu})^2 = 5.6 \times 10^{-8}$, and $(s_L^{\nu \tau})^2 = 0.01$. A full description of each figure is given in the text, together with the interpretation of the results presented by the curves shown in the figure. To avoid ambiguities, where they could emerge, the curves in the figures are designated or characterized in two ways — with letters and by type and weight of the line.

Figure 1 shows the dependence of upper bounds of branching ratios (UBBRs) on the heavy-neutrino mass, in the case of degenerate neutrino masses $m_{N_i} = m_N$, $i=1, \dots, n_R$. The letters a, b, c, d, e, f, and g designate the UBBRs for $K_L \rightarrow e^- \mu^+$, $\pi^0 \rightarrow e^- \mu^+$, $\eta \rightarrow e^- \mu^+$, $K^+ \rightarrow \pi^+ e^- \mu^+$, $\Sigma^+ \rightarrow p e^- \mu^+$, $\Sigma^0 \rightarrow n e^- \mu^+$, and $\Lambda \rightarrow e^- \mu^+$, respectively. Left and right diagrams of the figure show the results obtained in models Vn_R , $n_R=2,4$, and models An_R , $n_R=2,4$, respectively. The thick (thin) lines are results obtained for $n_R=2$ ($n_R=4$). The m_N domain in the Vn_R model is larger by a factor of $\sqrt{2}$ than in the An_R model. The m_N domain in the $n_R=4$ model is larger by a factor of $\sqrt{2}$ than in the $n_R=2$ model from the same class of models. Concerning the m_N dependence, UBBRs for LFV processes studied here may be divided into two groups, the group of processes having only a box contribution to the amplitude, and the group having box and Z-boson exchange contributions. The UBBRs within these groups have a very similar m_N dependence. The UBBRs in the Vn_R models are independent of n_R

TABLE II. The values for maximal UBBRs for degenerate heavy-neutrino masses and for two sets of $(s_L^{\nu_l})^2$ mixings: for maximal mixings and for $(s_L^{\nu_e})^2=0.00355$, $(s_L^{\nu_\tau})^2=0.03$, and $(s_L^{\nu_e})^2(s_L^{\nu_\mu})^2=2.8\times 10^{-8}$ (results in brackets).

Model	V2	V4	A2	A4
$(m_N)_{max}$ (GeV)	9500 (6800)	13400 (9600)	6700 (4800)	9500 (6800)
$K_L \rightarrow e^- \mu^+$	2.9×10^{-16} (1.3×10^{-16})	3.3×10^{-16} (1.5×10^{-16})	2.6×10^{-16} (1.1×10^{-16})	2.9×10^{-16} (1.3×10^{-16})
$\pi^0 \rightarrow e^- \mu^+$	3.2×10^{-16} (1.4×10^{-16})	1.4×10^{-15} (6.3×10^{-16})	2.9×10^{-18} (1.4×10^{-18})	3.2×10^{-16} (1.4×10^{-16})
$\eta \rightarrow e^- \mu^+$	7.5×10^{-18} (3.4×10^{-18})	3.2×10^{-17} (1.5×10^{-17})	7.5×10^{-20} (3.5×10^{-20})	7.5×10^{-18} (3.4×10^{-18})
$K^+ \rightarrow \pi^+ e^- \mu^+$	3.7×10^{-18} (1.7×10^{-18})	4.2×10^{-18} (1.9×10^{-18})	3.2×10^{-18} (1.4×10^{-18})	3.7×10^{-18} (1.7×10^{-18})
$\Sigma^+ \rightarrow p e^- \mu^+$	1.8×10^{-20} (7.8×10^{-21})	2.0×10^{-20} (8.9×10^{-21})	1.6×10^{-20} (6.8×10^{-21})	1.8×10^{-20} (7.8×10^{-21})
$\Xi^0 \rightarrow \Lambda e^- \mu^+$	1.7×10^{-20} (7.6×10^{-21})	2.0×10^{-20} (8.7×10^{-21})	1.5×10^{-20} (6.7×10^{-21})	1.7×10^{-20} (7.6×10^{-21})
$\Sigma^0 \rightarrow n e^- \mu^+$	1.1×10^{-20} (4.8×10^{-21})	1.2×10^{-20} (5.5×10^{-21})	9.5×10^{-21} (4.2×10^{-21})	1.1×10^{-20} (4.8×10^{-21})

(the thick and thin lines coincide), and have a very similar m_N dependence as the UBBRs in the A4 model. The UBBRs in the An_R models depend on n_R . That dependence is weak in processes whose amplitudes have box contribution to the amplitude only, but is very strong if the amplitude of the process contains a Z-boson exchange contribution. This strong dependence is a consequence of the *special form* of B matrices in the A2 model. For degenerate heavy-neutrino masses, the special form of B matrices leads to the zero contribution of the $H_Z(x,y)$ loop function to the amplitudes. In all other An_R models and in all Vn_R models, the $H_Z(x,y)$ loop function gives a maximal contribution. Namely, the B matrix elements are unknown, and, therefore, the products of the B matrix elements have to be replaced by the largest value they can assume. That explains the ~ 25 times larger UBBRs in the A4 model than in the A2 model at $m_N = 6700$ GeV.

For degenerate heavy-neutrino masses, the maximal values for UBBRs for the most interesting LFV leptonic meson decays, LFV semileptonic meson decays, and semileptonic baryon decays are given in Table II for two sets of $(s_L^{\nu_l})^2$ mixings. Among the decays having a box amplitude only (box and Z-boson exchange amplitudes), the $K_L \rightarrow e^- \mu^+$ ($\pi^0 \rightarrow e^- \mu^+$) decay has the largest UBBR. In the following discussion, only these two processes will be studied. It is interesting that in models V2, V4 and A4, the $\pi^0 \rightarrow e^- \mu^+$ may have larger UBBRs than $K_L \rightarrow e^- \mu^+$, despite the π^0 meson having a much larger total decay rate than the K_L meson. That makes $\pi^0 \rightarrow e^- \mu^+$ decay interesting for experimental studies of lepton-flavor violation. In models with a larger n_R , the ratio of maximal UBBRs for $\pi^0 \rightarrow e^- \mu^+$ and $K_L \rightarrow e^- \mu^+$ decays is larger.

The maximum values for UBBRs are not obtained for equal heavy-neutrino masses. For instance, in the V2 model, if one of the masses is larger by the factor ρ_2 than the other, the maximum for $\pi^0 \rightarrow e^- \mu^+$ is reached at $\rho_2 = 1.85$, and it

is 7.7 times larger than the corresponding maximum value given in Table II. Similarly, the maximum UBBR value for $K_L \rightarrow e^- \mu^+$ decay in the V2 model is obtained for $\rho_2 = 5.3$ and it is equal 5.0×10^{-16} . The maximum UBBR values for $\pi^0 \rightarrow e^- \mu^+$ decay in V3 and V4 models are found at $\rho_2 = 1.6$ and $\rho_2 = 1.5$, respectively, and they are equal to 4.34×10^{-15} and 6.41×10^{-15} . The maximum UBBR values for $K_L \rightarrow e^- \mu^+$ decay in V3 and V4 models are reached at $\rho_2 = 4.5$ and $\rho_2 = 4.1$ and they are equal to 5.04×10^{-16} and 5.11×10^{-16} , respectively. Notice that the maximum UBBR value for $K_L \rightarrow e^- \mu^+$ decay almost does not depend on the number of heavy neutrinos, while the maximum UBBR value for $\pi^0 \rightarrow e^- \mu^+$ decay has an almost linear dependence on n_R . For larger n_R values, we expect a weaker n_R dependence of the maximum UBBR value for $\pi^0 \rightarrow e^- \mu^+$ decay.

Figure 2 compares the m_{N_1} dependence of UBBRs for $K_L \rightarrow e^- \mu^+$ and $\pi^0 \rightarrow e^- \mu^+$ decays for different ρ_2 values evaluated in models V2 and A2. The letters a, b, c, d, e, f, g, h, and i correspond to the ρ_2 values 1, 3, 10, 30, 100, 300, 1000, 3000, and 10000, respectively. In the right diagrams of Figs. 2a and 2b the curves strongly overlap, and, therefore, only curves belonging to ρ_2 values 1, 3, 10, and 300 are marked at the end points of the curves. The left and right diagrams of the figures show the results of the V2 and A2 models, respectively. Figures 2a and 2b show the results for $K_L \rightarrow e^- \mu^+$ decay and $\pi^0 \rightarrow e^- \mu^+$ decay, respectively. The UBBR curves for $K_L \rightarrow e^- \mu^+$ and $\pi^0 \rightarrow e^- \mu^+$, evaluated in the V2 model for $\rho_2 \neq 1$, lie above the $\rho_2 = 1$ curves. As the ρ_2 increases, the UBBR curves first tend to separate from the $\rho_2 = 1$ curves, and then, after ρ_2 reaches some critical value, begin to approach back to the $\rho_2 = 1$ curves. As the ρ_2 tends to infinity the UBBR curves cannot be distinguished from the $\rho_2 = 1$ curves. This behavior is a manifestation of the decoupling of very heavy neutrinos from the light particles. The second interesting effect in the UBBR curves is the appearance of peaks at which the UBBR curves break. The UBBR

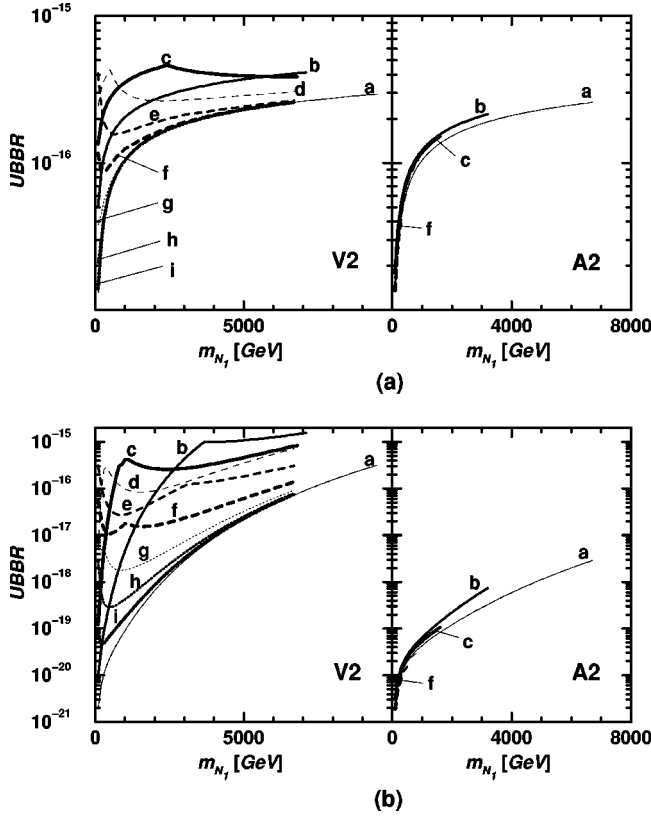


FIG. 2. The UBBRs for $K_L \rightarrow e\mu$ and $\pi^0 \rightarrow e\mu$ decays versus m_{N_1} for several ρ_2 values in models V2 and A2.

curves of $K_L \rightarrow e^- \mu^+$ decay show one one peak, while the UBBR curves of $\pi^0 \rightarrow e^- \mu^+$ decays show two peaks. The peaks emerge at some ρ_2 value, and as ρ_2 increases they move towards $m_{N_1} = 0$, and disappear. These peaks occur at or above the m_{N_1} values at which some of the upper bounds on B_{IN_i} matrix elements begin to be evaluated using Eq. (19). Starting from $\rho_2 = 1$, the ρ_2 value increases and the domain of m_{N_1} values becomes smaller, but for $\rho_2 \gtrsim 30$, the maximal m_{N_1} value is almost independent of ρ_2 . Notice that the maximal values for UBBRs are not reached at the largest m_{N_1} value on the $\rho_2 = 1$ curve, but at the peak (first peak for $\pi^0 \rightarrow e^- \mu^+$ decay) for $\rho_2 \approx 5$. As mentioned, the maximum UBBR value for $K_L \rightarrow e^- \mu^+$ and $\pi^0 \rightarrow e^- \mu^+$ is ~ 2 and ~ 7 times larger than the maximum UBBR at the largest m_{N_1} value on the $\rho_2 = 1$ curve. The UBBR curves for $K_L \rightarrow e^- \mu^+$ and $\pi^0 \rightarrow e^- \mu^+$ evaluated in the A2 model do not have peaks, because in this model only the upper bound (16) is imposed on the heavy-neutrino masses. As ρ_2 increases, the domain of the m_{N_1} values quickly reduces, and at some critical ρ_2 value it disappears. That is, the ρ_2 domain is bounded, too. For ρ_2 smaller than this critical value, the UBBR curves show similar ‘‘decoupling’’ behavior—as ρ_2 increases, for $\rho_2 \lesssim 3$ the curves move away from the $\rho_2 = 1$ curve, and for $\rho_2 \gtrsim 3$ move toward it. The ρ_2 dependence of this ‘‘decoupling’’ is much weaker than in other models—the UBBR curves almost overlap. As the domain of the ρ_2 values is finite one cannot truly talk about the decoupling of very heavy neutrinos.

Figure 3 compares the dependence of UBBRs for K_L

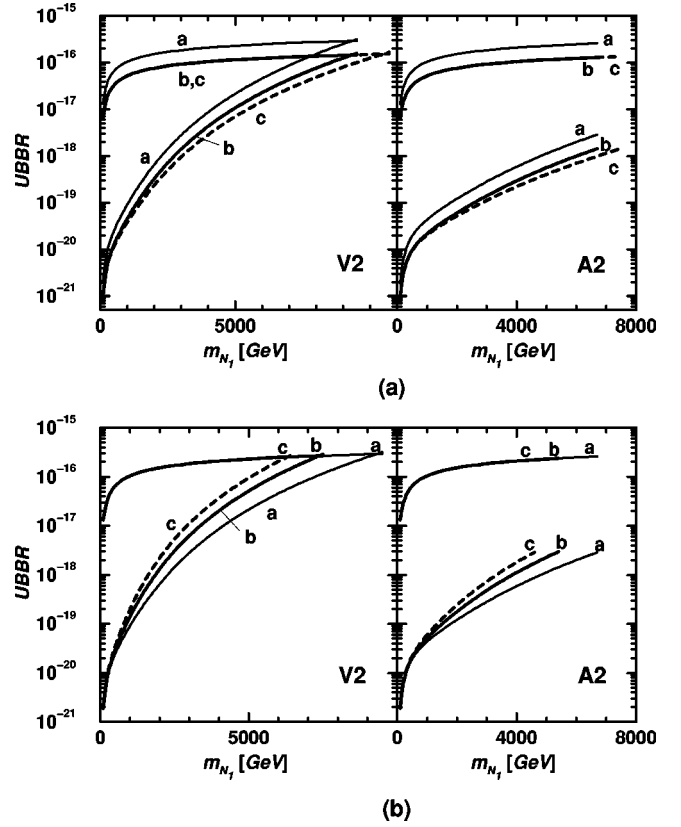


FIG. 3. The UBBRs for $K_L \rightarrow e\mu$ and $\pi^0 \rightarrow e\mu$ decays versus m_{N_1} for several $(s_L^{\nu_e})^2$ and $(s_L^{\nu_\tau})^2$ values in models V2 and A2.

$\rightarrow e^- \mu^+$ and $\pi^0 \rightarrow e^- \mu^+$ decays on $m_N = m_{N_i}$ for several values of the squares of mixing parameters $(s_L^{\nu_i})^2$. The less inclined lines correspond to $K_L \rightarrow e^- \mu^+$ decay while the steeper lines represent $\pi^0 \rightarrow e^- \mu^+$ decay. The curves in the left diagrams of Figs. 3a and 3b are found in V2 and A2 models, respectively. Figure 3a gives the UBBR curves for $(s_L^{\nu_\tau})^2 = 0.01$ and three pairs of $((s_L^{\nu_e})^2, (s_L^{\nu_\mu})^2, (s_L^{\nu_\tau})^2)$ values, $(0.0071, 5.6 \times 10^{-8})$, $(0.0071, 2.8 \times 10^{-8})$ and $(0.00355, 2.8 \times 10^{-8})$, denoted by a (solid line), b (solid gray line), and c (dashed line), respectively. Figure 3b represents the UBBRs for $(s_L^{\nu_e})^2 = 0.0071$, $(s_L^{\nu_\mu})^2 = 5.6 \times 10^{-8}$ and three $(s_L^{\nu_\tau})^2$ values, $(s_L^{\nu_\tau})^2 = 0.01$, $(s_L^{\nu_\tau})^2 = 0.02$, and $(s_L^{\nu_\tau})^2 = 0.03$, designated by a (solid line), b (solid gray line), and c (dashed line), respectively. The figures show that the UBBRs for $K_L \rightarrow e^- \mu^+$ depend only on the product of mixings $(s_L^{\nu_e})^2 (s_L^{\nu_\nu})^2$ (b and c curves in Fig. 3a coincide, and a , b , and c curves in Fig. 3b coincide). The $\pi^0 \rightarrow e^- \mu^+$ curves depend on all $(s_L^{\nu_i})^2$ parameters. A decrease (increase) of the parameter $(s_L^{\nu_e})^2$ or $(s_L^{\nu_\tau})^2$ leads to a larger (smaller) m_N domain. The maximal UBBR value for $\pi^0 \rightarrow e^- \mu^+$ decay slightly decreases (slightly increases) in the V2 (A2) model as $(s_L^{\nu_\tau})^2$ or $(s_L^{\nu_e})^2$ increases. It is interesting that in the V2 model $K_L \rightarrow e^- \mu^+$ and $\pi^0 \rightarrow e^- \mu^+$ curves always cross almost at the maximum m_{N_1} value for any particular values of the mixing parameters. As we will see in Fig. 5, only the ρ_2 value changes that property, that is, changes the intersection point (or relative position) of $K_L \rightarrow e^- \mu^+$ and $\pi^0 \rightarrow e^- \mu^+$ curves.

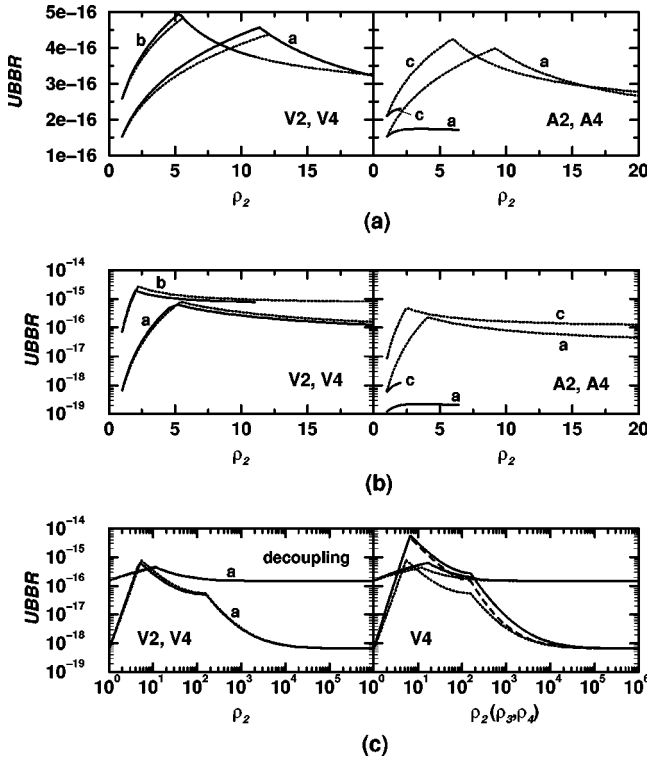


FIG. 4. The UBBRs for $K_L \rightarrow e\mu$ and $\pi^0 \rightarrow e\mu$ decays versus ratios $\rho_i = m_{N_i}/m_N$ for several m_{N_i} values in models V2, V4, A2, and A4.

Figure 4 presents the dependence of the UBBRs on the ratios ρ_i , $i=2,3,4$, in the models V2, V4, A2, and A4. Figures 4a and 4b compares the ρ_2 dependence of UBBRs of $K_L \rightarrow e^- \mu^+$ and $\pi^0 \rightarrow e^- \mu^+$ decays, respectively, in Vn_R models and An_R models, assuming that $m_{N_1} = m_{N_3} = m_{N_4}$. The solid (dotted) lines represent the results in models with two (four) heavy neutrinos. The letters a, b, and c denote curves obtained for $m_{N_1} = 2000$ GeV, $m_{N_1} = 6700$ GeV, and

$m_{N_1} = 4000$ GeV, respectively. The results given in the left diagrams of Figs. 4a and 4b are obtained in Vn_R (V2 and V4) models, while those on the right diagrams are obtained in An_R (A2 and A4) models. In Fig. 4c, the behavior of UBBRs for both $K_L \rightarrow e^- \mu^+$ and $\pi^0 \rightarrow e^- \mu^+$ decays are shown together, but in a much larger ρ_i domain. The main idea of this figure is to show the *decoupling* of very heavy neutrinos from light particles. Both the left and right diagrams of Fig. 4c present only the results for $m_{N_1} = 2000$ GeV. The left diagram of Fig. 4c is an enlarged version of the results in the left diagrams of Figs. 4a and 4b for $m_{N_1} = 2000$ GeV. The letter destinations and the meaning of the types of curves in the left diagram of Fig. 4c are the same as in Figs. 4a and 4b, and it is also assumed that $m_{N_1} = m_{N_3} = m_{N_4}$. The right diagram of Fig. 4c shows only the results in the V4 model, but for one, two or three neutrinos with increasing mass, corresponding to $m_{N_1} = m_{N_3} = m_{N_4}$ and $m_{N_2} = m_{N_1} \times \rho_2$ (dotted line), $m_{N_1} = m_{N_4}$ and $m_{N_2} = m_{N_3} = m_{N_1} \times \rho_2$ (gray line), and $m_{N_2} = m_{N_3} = m_{N_4} = m_{N_1} \times \rho_2$ (dashed line). Having defined the notation, we can now proceed with the discussion of the results shown in Fig. 4. The results obtained in the A2 model differ considerably from the results of other models. In the A2 model, the domain of ρ_2 values is finite and strongly depends on m_{N_1} . The UBBR values in the A2 model are smaller than in other models, slightly for $K_L \rightarrow e^- \mu^+$ decay (for decays depending on box amplitude only) and considerably for $\pi^0 \rightarrow e^- \mu^+$ decay (for decays with Z-boson exchange amplitude). The UBBR curves are smooth, increase slower than in other models, and in the case of decays with a Z-boson exchange amplitude often have a maximum [20,26]. The UBBR curves corresponding to the larger m_{N_1} lie above those evaluated for smaller m_{N_1} . In other models (represented by V2, V4, and A4 models in Fig. 4), the ρ_2 domain extends from one to infinity. Every UBBR curve has two peaks. One is at the ρ_2 value at which the use

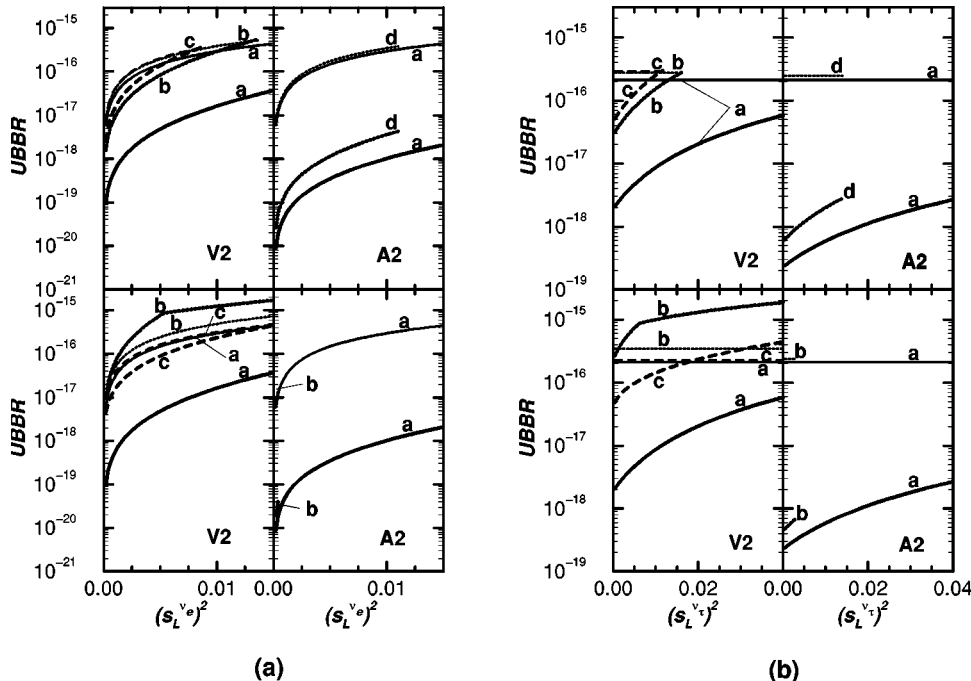


FIG. 5. The UBBRs for $K_L \rightarrow e\mu$ and $\pi^0 \rightarrow e\mu$ decays versus $(s_L^{nu e})^2$ and $(s_L^{nu tau})^2$ for several m_{N_i} values and several ρ_2 values in models V2 and A2.

of upper limits for the loop form factors (B9) starts to give smaller UBBR value than the upper limits (B8). The other is at the point at which $B_{\mu N_i}^1$ becomes smaller than $B_{\mu N_i}^0$. The second peak is visible only in processes depending on a Z-boson exchange amplitude. Namely, in the box amplitudes, the ρ_2 value at the second peak is so large that the part of the amplitude depending on the mass m_{N_2} is negligible. The UBBR curves in Vn_R models are almost independent of n_R , but they depend on m_{N_1} . Namely, the position of both peaks strongly depends on m_{N_1} . Generally, the UBBR curves corresponding to the larger m_{N_1} values lie above those evaluated for smaller m_{N_1} . In the models with $n_R > 2$ the UBBRs depend significantly on the number of very heavy neutrinos in the ranges $10 \lesssim \rho_2 \lesssim 150$ and $5 \gtrsim \rho_2 \gtrsim 20\,000$ for decays depending on a box amplitude only and on box and Z-boson exchange amplitudes, respectively. For any process, the UBBR for $\rho_2 \rightarrow \infty$ and the UBBR at $\rho_2 = 1$ are equal. As the upper bound on the UBBR terms depending on masses satisfying $m_{N_i} \approx m_{N_1}$ is constructed using Schwartz's inequality (B4), these UBBR terms are equal at $\rho_2 = 1$ and for $\rho_2 \rightarrow \infty$, showing that UBBR term depending on m_{N_2} becomes equal to zero in the $\rho_2 \rightarrow \infty$ limit. This is a manifestation of decoupling of heavy particles from the light sector of the model. In processes depending on box amplitudes only, the heavy neutrinos decouple faster than in processes depending on box and Z-boson exchange amplitudes. For example, for the parameters of Fig. 4c, UBBRs of $K_L \rightarrow e^- \mu^+$ and $\pi^0 \rightarrow e^- \mu^+$ decays reach 10% larger value than UBBRs at $\rho_2 = 1$ at $\rho_2 = 200$ and $\rho_2 = 33\,000$, respectively. The slow decoupling of heavy neutrinos in processes depending on Z-boson exchange amplitudes is a consequence of mixing amplitude terms, containing heavy (m_{N_2}) and light ($m_{N_i}, i \neq 2$) heavy neutrinos. The processes depending on Z-boson exchange amplitudes illustrate that the *nondecoupling window*, that is, the region of mass parameters where large heavy-neutrino masses have a considerable effect on the amplitude, heavily depends on the structure of the amplitude of the process, and that it may extend over several orders of magnitude of heavy-neutrino masses. The UBBR curves in An_R , $n_R \neq 2$, models have the same properties as the UBBR curves in Vn_R models.

Figures 5a and 5b give the dependence of UBBRs on squares of the mixing parameters $(s_L^{\nu e})^2$ and $(s_L^{\nu \tau})^2$, respectively. The thinner lines represent the results for $K_L \rightarrow e^- \mu^+$ decay, and the thick ones the results for $\pi^0 \rightarrow e^- \mu^+$ decay. The left two diagrams in Fig. 5a and Fig. 5b were evaluated in the model V2, while the right ones were obtained in the model A2. The upper two diagrams of Fig. 5a and Fig. 5b show the $(s_L^{\nu e})^2$ and $(s_L^{\nu \tau})^2$ dependence of UBBRs, respectively, for $m_N = m_{N_1} = m_{N_2}$ values 2000 GeV (a, solid lines), 6000 GeV (d, dotted lines), 8000 GeV (b, dotted lines), and 9000 GeV (c, dashed lines). The lower two diagrams of Fig. 5a and Fig. 5b compare the $(s_L^{\nu e})^2$ and $(s_L^{\nu \tau})^2$ dependence of UBBRs, respectively, for $\rho_2 = 1$ (a, solid lines), $\rho_2 = 3$ (b, dotted lines), and $\rho_2 = 100$ (c, dashed lines). As expected from the structure of the amplitudes, the results show that the UBBRs comprising the box diagram amplitude

only do not depend on $(s_L^{\nu \tau})^2$, and have a linear $(s_L^{\nu e})^2$ dependence for almost all m_{N_1} and ρ_2 values. The slight deviation from the linear $(s_L^{\nu e})^2$ dependence is found only in the curve evaluated for $\rho_2 = 100$. The UBBRs having Z-boson exchange amplitudes show something between linear and cubic $(s_L^{\nu e})^2$ dependence, and between $(s_L^{\nu \tau})^2$ independence and quadratic $(s_L^{\nu \tau})^2$ dependence. This behavior is expected from the structure of the amplitudes. The deviations from the smooth $(s_L^{\nu \tau})^2$ and $(s_L^{\nu e})^2$ behavior (peaks) of curves evaluated for $\rho_2 \neq 1$ is a consequence of passing through the $(s_L^{\nu i})^2$ values, at which the the matrix element B_{IN_i} of the heavier of two heavy neutrinos begins to satisfy the $s_L^{\nu i}$ -independent upper bound (19). For the same reason, a departure from the linear $(s_L^{\nu e})^2$ dependence in the $K_L \rightarrow e^- \mu^+$ curve appears. The upper four diagrams of Figs. 5a and 5b show how the $(s_L^{\nu e})^2$ and $(s_L^{\nu \tau})^2$ domains reduce as m_N enlarges. Beyond the maximal m_N values, defined in Eqs. (17) and (16), the curves do not exist. The lower four diagrams of Figs. 5a and 5b manifest the difference between A2 and V2 models (all other models) concerning the ρ_2 dependence. In the A2 model, the ρ_2 domain depends on ρ_2 considerably. For ρ_2 not satisfying Eq. (16) the curves do not exist. In the V2 model (all other models), the $(s_L^{\nu e})^2$ and $(s_L^{\nu \tau})^2$ UBBR curves exist for any ρ_2 value, if $m_{N_1} \leq m_{N_1}^0$. In the left two of the lower diagrams one can follow how the $\rho_2 \neq 1$ curves, for ascending ρ_2 , depart from the $\rho_2 = 1$ curve for small ρ_2 values, and approach it back as $\rho_2 \rightarrow \infty$. These results, together with the similar behavior of m_{N_1} curves, shown in Figs. 2a and 2b, show that the decoupling of very heavy neutrinos occurs for all allowed values of the remaining free-parameter space.

VII. SUMMARY AND CONCLUSION

LFV decays of light hadrons have been studied and evaluated in extensions of the standard model with heavy Dirac (Vn_R models) and Majorana (An_R models) neutrinos. The expressions for perturbative unitarity bounds on heavy neutrino masses were found to have the same form in Vn_R models and An_R , $n_R \neq 2$, models, but are different from the perturbative unitarity bound in the A2 model. The difference comes from the *different number of free parameters* defining the B and C matrices. The perturbative unitarity bounds lead to the bounded space of heavy-mass values in A2 models, while in other models all heavy-neutrino masses, except the lightest one, may assume any value. More precisely, the perturbative unitarity bounds on all masses, except the lightest one, do not constrain a heavy-neutrino mass, but the product of the heavy-neutrino mass m_{N_i} and absolute value of a B_{IN_i} matrix element. So the enlargement of a specific heavy-neutrino mass to infinity leads to a zero value for the B_{IN_i} matrix elements. The minimal value of the lightest heavy-neutrino mass is bounded in all models. In An_R , $n_R \neq 2$, models and Vn_R models, the maximal value of the lightest heavy-neutrino mass depends considerably on the number of heavy neutrinos n_R .

The infinite domain of heavy-neutrino masses in Vn_R and An_R , $n_R \neq 2$, models gives the possibility of explicit study of

the *decoupling* of very heavy-neutrinos from the lighter particles [35] in the model, looking for the mass dependence of the branching ratios in the limit of very large heavy neutrino mass values. For such a study, explicit expressions for the branching ratios for processes depending on heavy neutrinos, or at least the upper bounds on the branching ratios, must be found. In fact, only the upper bounds on the branching ratios of such decays may be found, because the B matrices are not explicitly known in models with an infinite heavy-neutrino mass domain. The upper bounds of branching ratios (UBBRs) for LFV decays of light hadrons were found in this paper. This was done using a combination of Schwartz's inequalities for sums containing either B_{IN} matrix elements or matrix elements of the Kobayashi-Maskawa matrix. Specifically, if the matrix elements in a sum were unknown, and their absolute values were expected to be of the same order of magnitude, the usual Schwartz's inequality was used. If any of the matrix elements was known to have a smaller absolute value than others in the sum, the term containing it was extracted, replaced by its absolute value, and the rest of the sum evaluated using Schwartz's inequality. If any of the parameters which influence the absolute value of any matrix element appearing in the sum changes continuously, such a procedure leads to discontinuous UBBR curves at points where the matrix element becomes "small." For that reason at the parameter points at which the discontinuity would occur the UBBR values were evaluated with and without extraction of the term containing a "small" matrix element, and the smaller of the two values was taken as the UBBR at that point. In such a way the discontinuities were removed, but the UBBR curves gain peaks. The peaks are artifacts of our "upper bound" procedure. Nevertheless, they are helpful in discussions, because each peak tags one point on the UBBR curves, and, therefore, one can follow the mapping of points in the UBBR curves as any of the free parameters changes. Using the UBBRs obtained in such a way, we found that the very heavy neutrinos decouple in the infinite mass limit, and that is valid for all values of the remaining free-parameter space, when one or more masses tend to infinity. There is one more interesting property of UBBR curves concerning decoupling and "nondecoupling" of heavy neutrinos. The region of heavy-neutrino masses in which the heavy neutrinos have a large effect on the decay rate, the so-called *nodecoupling window*, may be very large, and it strongly depends on the *structure* of the amplitude of the process. In processes with a Z -boson exchange amplitude it extends over four to five orders of magnitude in heavy-neutrino mass(es), while in processes depending on a box amplitude only, the dependence extends over two orders of magnitude of heavy-neutrino mass(es). So large "nondecoupling" windows may make the decoupling of heavy particles *ineffective* in the experimentally interesting regions of parameter space.

The UBBR curves, obtained with the above procedure, have a few more nice properties. In the case of degenerate neutrinos, the UBBRs as functions of m_N are independent of n_R , although the maximum m_N values depend on n_R . If one mass increases and the others are kept constant, the UBBRs are almost independent of n_R . Further, the curves for UBBRs for decays containing a box diagram amplitude only are slightly larger than the corresponding curves obtained in

the $A2$ model. That shows that the upper bounds obtained in Vn_R and An_R , $n_R \neq 2$, models approximate the expressions obtained in a model with exact expressions for B matrices very well. The UBBRs dependent on the Z -boson exchange amplitudes differ considerably from the corresponding curves in the $A2$ model, but that can be explained by the specific phase structure of B matrices which makes the contribution of the largest loop function in the Z -boson amplitude equal to zero. The unknown phase structure of B_{IN} matrix elements in Vn_R and An_R , $n_R \neq 2$, models makes the largest loop function contribution in the Z -boson amplitude the dominant one. This makes the processes having the Z -boson contribution more interesting than in the $A2$ model, from the experimental point of view. Next, all UBBR curves obtained in Vn_R and An_R , $n_R \neq 2$, models lie above the corresponding curves in the $A2$ models. In fact, the UBBRs we obtained give the upper bounds for the branching ratios for *any extension of standard model with heavy neutrinos*, with B and C matrices satisfying relations (6).

Concerning the hadron part of the LFV amplitudes of hadron decays, they were evaluated in standard ways. For the pseudoscalar meson to vacuum matrix element, partially conserved axial-vector current (PCAC) was used. The pseudoscalar-to-pseudoscalar matrix elements were evaluated in two ways. The first evaluation is based on the chiral Lagrangian extended by vector mesons, while the other one uses the form factor decomposition of the pseudoscalar-to-pseudoscalar matrix element. The first approach gives a somewhat too large a value for the form factor f_+ at the zero momentum transfer, but allows one to show that the matrix element $K_L \rightarrow \pi^0$ is equal to zero. In the second one, the $f_+(0)$ is extracted from the experiment, but the $K_L \rightarrow \pi^0$ matrix element cannot be evaluated. After renormalizing the $f_+(0)$ to the value obtained in the second approach, the first one gives almost the same values for $K^+ \rightarrow \pi^+ e^- \mu^+$ UBBRs as the second one. The baryon-to-baryon matrix elements were evaluated using the form factor decomposition of generic matrix elements, $SU(3)$ -flavor symmetry to connect charge f_1 and axial charge g_1 form factors, and Goldberger-Treiman relation for finding effective pseudoscalar form factors g_3 from g_1 form factors. The effective scalar form factor f_3 and weak electricity form factor g_2 were neglected since corresponding terms violate G parity, and the weak magnetism form factor f_2 was estimated to give a negligible contribution to the hadron amplitude. These baryon-to-baryon matrix elements may be found in standard books and, in the context of LFV in baryon decays, were evaluated before, including f_2 form factors [32].

From the experimental point of view, the leptonic LFV decays of mesons are most interesting, specifically the decays $K_L \rightarrow e^- \mu^+$ and $\pi^0 \rightarrow e^- \mu^+$. Namely, the maximal UBBRs for semileptonic LFV decays of mesons and baryons are smaller than $\sim 10^{-17}$ and $\sim 10^{-20}$, respectively. The maximal UBBRs for decays $K_L \rightarrow e^- \mu^+$ and $\pi^0 \rightarrow e^- \mu^+$ may reach values as large as $\sim 5 \times 10^{-16}$ and $\leq (2n_R - 2) \times 10^{-15}$, respectively. These results are still several orders of magnitude below the present experimental upper limits. The maximal results depend on the type of the model. They are larger in the models with more heavy neutrinos. They are larger in Vn_R models than in An_R models. As far as we

know, only $K_L \rightarrow e^- \mu^+$ decay was extensively studied. We would like to stress that the ‘‘nondecoupling’’ effects, appearing in processes comprising the Z-boson exchange amplitude, could make the $\pi^0 \rightarrow e^- \mu^+$ decay *equally interesting* for experimental study of lepton-flavor violation as $K_L \rightarrow e^- \mu^+$ decay. The UBBR for $\pi^0 \rightarrow e^- \mu^+$ may be an order of magnitude larger than the UBBR for $K_L \rightarrow e^- \mu^+$ decay.

ACKNOWLEDGMENTS

We wish to thank to Marijan Mileković for a careful reading of the manuscript. This work is supported by project 1-03-233 ‘‘Field theory and structure of elementary particles’’ and the DLR-Internationales Büro, under project number 6B0A1A.

APPENDIX A: FORM FACTORS AND LOOP FUNCTIONS

The composite form factors $a_P^{\mu e}$, $a_{K^+ \pi^+}^{\mu e}$, and $a_{BB'}^{\mu e}$, given in Eqs. (22), (26), and (39), respectively, are defined in terms of composite form factors $F_Z^{\mu e}$, $F_{box}^{\tau l' d_a d_b}$, and $F_{box}^{\tau l' d_a d_b}$ which are listed here for the convenience of the reader:

$$\begin{aligned}
F_Z^{\mu e} &= \sum_{i,j=1}^{n_R} B_{\mu N_i}^* B_{e N_j} [\delta_{N_i N_j} (F_Z(\lambda_{N_i}) + 2G_Z(0, \lambda_{N_i})) \\
&\quad + C_{N_i N_j}^* (G_Z(\lambda_{N_i}, \lambda_{N_j}) - G_Z(0, \lambda_{N_i}) - G_Z(0, \lambda_{N_j})) \\
&\quad + C_{N_i N_j} H_Z(\lambda_{N_i}, \lambda_{N_j})], \\
F_{box}^{\mu e uu} &= \sum_{i=1}^{n_R} \sum_{j=1}^{n_G} B_{\mu N_i}^* B_{e N_j} V_{ud_j}^* V_{ud_j} [H_{box}(\lambda_{N_i}, \lambda_{d_j}) \\
&\quad - H_{box}(\lambda_{N_i}, 0) - H_{box}(0, \lambda_{d_j}) + H_{box}(0, 0)] \\
&\quad + \sum_{i=1}^{n_R} B_{\tau N_i}^* B_{l' N_i} [H_{box}(\lambda_{N_i}, 0) - H_{box}(0, 0)], \\
F_{box}^{\mu e d_a d_b} &= \sum_{i=1}^{n_R} \sum_{j=1}^{n_G} B_{\mu N_i}^* B_{e N_j} V_{u_j d_a}^* V_{u_j d_b} [F_{box}(\lambda_{N_i}, \lambda_{d_j}) \\
&\quad - F_{box}(\lambda_{N_i}, 0) - F_{box}(0, \lambda_{d_j}) + F_{box}(0, 0)] \\
&\quad + \delta_{d_a d_b} \sum_{i=1}^{n_R} B_{\tau N_i}^* B_{l' N_i} [F_{box}(\lambda_{N_i}, 0) - F_{box}(0, 0)],
\end{aligned} \tag{A1}$$

where $\lambda_X = m_X^2/M_W^2$. The composite loop form factors are expressed in terms of the loop functions F_Z , G_Z , H_Z , F_{box} and H_{box} given by

$$\begin{aligned}
F_Z(x) &= -\frac{5x}{2(1-x)} - \frac{5x^2}{2(1-x)^2} \ln x, \\
G_Z(x, y) &= -\frac{1}{2(x-y)} \left[\frac{x^2(1-y)}{1-x} \ln x - \frac{y^2(1-x)}{1-y} \ln y \right],
\end{aligned}$$

$$\begin{aligned}
H_Z(x, y) &= \frac{\sqrt{xy}}{4(x-y)} \left[\frac{x^2-4x}{1-x} \ln x - \frac{y^2-4y}{1-y} \ln y \right], \\
F_{box}(x, y) &= \frac{1}{x-y} \left[\left(1 + \frac{xy}{4} \right) \left(\frac{1}{1-x} + \frac{x^2 \ln x}{(1-x)^2} - \frac{1}{1-y} \right. \right. \\
&\quad \left. \left. - \frac{y^2 \ln y}{(1-y)^2} \right) - 2xy \left(\frac{1}{1-x} + \frac{x \ln x}{(1-x)^2} - \frac{1}{1-y} \right. \right. \\
&\quad \left. \left. - \frac{y \ln y}{(1-y)^2} \right) \right], \\
H_{box}(x, y) &= \frac{1}{x-y} \left[\left(4 + \frac{xy}{4} \right) \left(\frac{1}{1-x} + \frac{x^2 \ln x}{(1-x)^2} - \frac{1}{1-y} \right. \right. \\
&\quad \left. \left. - \frac{y^2 \ln y}{(1-y)^2} \right) - 2xy \left(\frac{1}{1-x} + \frac{x \ln x}{(1-x)^2} - \frac{1}{1-y} \right. \right. \\
&\quad \left. \left. - \frac{y \ln y}{(1-y)^2} \right) \right].
\end{aligned} \tag{A2}$$

More details how these expressions can be derived may be found in Refs. [20,26].

APPENDIX B: SCHWARTZ'S INEQUALITIES AND UPPER BOUNDS ON FORM FACTORS

Let $\mathbf{a} = (a_1, \dots, a_n)$, $\mathbf{b} = (b_1, \dots, b_n)$, $\mathbf{c} = (c_1, \dots, c_n)$, ... be the vectors of an n -dimensional vector space. From Schwartz's inequality for any pair of these vectors,

$$|\mathbf{a} \cdot \mathbf{b}| \equiv \left| \sum_{i=1}^n a_i b_i \right| \leq \left(\sum_{i=1}^n |a_i|^2 \right)^{1/2} \left(\sum_{j=1}^n |b_j|^2 \right)^{1/2} \equiv |\mathbf{a}| |\mathbf{b}|, \tag{B1}$$

one can derive the following inequalities:

$$|\mathbf{a} + \mathbf{b}| \leq |\mathbf{a}| + |\mathbf{b}|, \tag{B2}$$

$$\begin{aligned}
\left| \sum_{i=1}^n a_i b_i c_i \right| &\leq \left(\sum_{i=1}^n |a_i|^2 \right)^{1/2} \left(\sum_{j=1}^n |b_j|^2 \right)^{1/2} \left(\sum_{k=1}^n |c_k|^2 \right)^{1/2} \\
&\equiv |\mathbf{a}| |\mathbf{b}| |\mathbf{c}|,
\end{aligned} \tag{B3}$$

$$\left| \sum_{i=1}^n a_i b_i c_i \right| \leq |\mathbf{a}| |\mathbf{b}| \langle c \rangle + |\mathbf{a}| |\mathbf{b}| \left(\sum_{i=1}^n |c_i - \langle c \rangle|^2 \right)^{1/2}, \tag{B4}$$

where $\langle c \rangle = \sum_{i=1}^n c_i / n$. The obvious inequality

$$\left| \sum_{i=1}^n a_i b_i \right| \leq \sum_{i=1}^n |a_i| |b_i| \tag{B5}$$

may be understood as a special form of the inequality (B2). Using the above-derived inequalities, one can write down the upper limits on absolute values of composite form factors defined in Eqs. (22), (26), and (39). The absolute values of

composite form factors may be written in terms of absolute values of composite loop form factors,

$$\begin{aligned}
|a_{p0}^{\mu e}| &\leq \frac{\alpha_W^2}{16M_W^2} f_{p0} \left[|\alpha_Z| |F_Z^{\mu e}| + |\alpha_{box}^{uu}| |F_{box}^{\mu e uu}| \right. \\
&\quad \left. + \sum_{d_a, d_b = d, s} |\alpha_{box}^{d_a d_b}| |F_{box}^{\mu e d_a d_b}| \right], \\
|a_{K^+ \pi^+}^{\mu e}| &= \frac{\alpha_W^2}{16M_W^2} |F_{box}^{\mu e sd}|, \\
|a_{BB'}^{\mu eds}| &= \frac{\alpha_W^2}{16M_W^2} |F_{box}^{\mu eds}|. \tag{B6}
\end{aligned}$$

Here only in the first relation is the inequality (B2) used. Introducing abbreviations for the combinations of the loop functions appearing in the composite loop form factors,

$$f_Z(x) = F_Z(x) + 2G(0, x),$$

$$g_Z(x, y) = G_Z(x, y) - G_Z(0, x) - G_Z(0, y),$$

$$h_Z(x, y) = H_Z(x, y),$$

$$f_{box}(x, y) = F_{box}(x, y) - F_{box}(x, 0) - F_{box}(0, y) + F_{box}(0, 0),$$

$$\tilde{f}_{box}(x) = F_{box}(x, 0) - F_{box}(0, 0),$$

$$\begin{aligned}
h_{box}(x, y) &= H_{box}(x, y) - H_{box}(x, 0) \\
&\quad - H_{box}(0, y) + H_{box}(0, 0),
\end{aligned}$$

$$\tilde{h}_{box}(x) = H_{box}(x, 0) - H_{box}(0, 0), \tag{B7}$$

and using the unequalities (B1), (B2), (B4), (B5) and definition (8) for $s_L^{v'l}$, one can derive the following upper limits on the absolute values of the composite loop form factors:

$$\begin{aligned}
|F_Z^{\mu e}| &\leq s_L^{v\mu} s_L^{v_e} \left[|\langle f_Z \rangle| + \left\{ \sum_{i=1}^{n_R} [f_Z(\lambda_{N_i}) - \langle f_Z \rangle]^2 \right\}^{1/2} \right] + s_L^{v\mu} s_L^{v_e} \sum_l (s_L^{v'l})^2 \left[|\langle g_Z \rangle| + 2 \left\{ \sum_{i=1}^{n_R} [\langle g_Z(\lambda_{N_i}) \rangle_N - \langle g_Z \rangle]^2 \right\}^{1/2} \right. \\
&\quad \left. + \left\{ \sum_{i,j=1}^{n_R} [g_Z(\lambda_{N_i}, \lambda_{N_j}) - \langle g_Z(\lambda_{N_i}) \rangle_N - \langle g_Z(\lambda_{N_j}) \rangle_N + \langle g_Z \rangle_N]^2 \right\}^{1/2} \right. \\
&\quad \left. + \left\{ \sum_{i,j=1}^{n_R} [h_Z(\lambda_{N_i}, \lambda_{N_j}) - \langle h_Z(\lambda_{N_i}) \rangle_N - \langle h_Z(\lambda_{N_j}) \rangle_N + \langle h_Z \rangle_N]^2 \right\}^{1/2} \right], \\
|F_{box}^{\mu e d_a d_b}| &\leq s_L^{v\mu} s_L^{v_e} \left(\delta_{d_a d_b} \left[|\langle \tilde{f}_{box} \rangle| + \left\{ \sum_{i=1}^{n_R} [\tilde{f}_{box}(\lambda_{N_i}) - \langle \tilde{f}_{box} \rangle]^2 \right\}^{1/2} \right] + \sum_{j=1}^{n_G} |V_{u_j d_a}| |V_{u_j d_b}| \left[\left\{ \sum_{i=1}^{n_R} [f_{box}(\lambda_{N_i}, \lambda_{u_j}) \right. \right. \right. \\
&\quad \left. \left. \left. - \langle f_{box}(\lambda_{u_j}) \rangle_N \right]^2 \right\}^{1/2} + |\langle f_{box}(\lambda_{u_j}) \rangle_N| \right] \right), \\
|F_{box}^{\mu e uu}| &\leq s_L^{v\mu} s_L^{v_e} \left[\left(|\langle \tilde{h}_{box} \rangle| + \left\{ \sum_{i=1}^{n_R} [\tilde{h}_{box}(\lambda_{N_i}) - \langle \tilde{h}_{box} \rangle]^2 \right\}^{1/2} \right) + \sum_{j=1}^{n_G} |V_{ud_j}| |V_{ud_j}| \left(\left\{ \sum_{i=1}^{n_R} [h_{box}(\lambda_{N_i}, \lambda_{d_j}) - \langle h_{box}(\lambda_{d_j}) \rangle_N]^2 \right\}^{1/2} \right. \right. \\
&\quad \left. \left. + |\langle h_{box}(\lambda_{d_j}) \rangle_N| \right) \right]. \tag{B8}
\end{aligned}$$

In the above inequalities, $\langle \cdot \rangle$ denotes the average over all indices on which the loop function depends, while $\langle \cdot \rangle_N$ denotes the average over heavy-neutrino indices only ($\langle f(\dots) \rangle_N = \sum_{i=1}^{n_R} f(\lambda_{N_i}, \dots) / n_R$). Here a comment is in order. The absolute values of the elements of CKM matrix elements are quite well known, and they differ in magnitude considerably. Therefore, the best inequality to use is (B5). Using relation (B4) and the unitarity of the CKM matrix instead of relation (B5) one can obtain a $\sim 10^7$ times larger result. On the other hand, the absolute values of the matrix elements of B matrices are crudely bounded by Eqs. (18) and (19). If all B matrix elements satisfy Eq. (18), the best inequality to use is (B4), and the best approximation to the loop form factors is (B8). If some B_{IN_i} matrix elements satisfy Eq. (19) and if the (19) bound is much smaller than the (18) bound, for these B_{IN_i} matrix elements it is much better to use inequality (B5). The inequality (B4) and approximation (B8) would lead to divergent results for absolute values of composite loop form factors in the limit $m_{N_i} \rightarrow \infty$ for any of m_{N_i} masses. Therefore, we have constructed the upper bounds of absolute values of composite loop form factors in which the sums over heavy neutrinos are divided into two groups, depending on which inequality B_{IN_i} satisfy. The part of a sum over heavy neutrinos satisfying the bound (18) is approximated using the inequality (B4), while for the rest of the sum the inequality (B5) is used. The upper bounds on composite loop form factors read

$$\begin{aligned}
|F_Z^{\mu e}| &\leq s_L^{\nu\mu} s_L^{\nu e} \left[|\langle f_Z \rangle_s| + \left\{ \sum_{i_s} [f_Z(\lambda_{N_{i_s}}) - \langle f_Z \rangle_s]^2 \right\}^{1/2} \right] + \sum_{i_b} B_{\mu N_{i_b}}^0 B_{e N_{i_b}}^0 |\tilde{f}_Z(\lambda_{N_{i_b}})| + s_L^{\nu\mu} s_L^{\nu e} \sum_l (s_L^{\nu l})^2 \left[|\langle g_Z \rangle_s| \right. \\
&\quad + 2 \left\{ \sum_{i_s} [\langle g_Z(\lambda_{N_{i_s}}) \rangle_{N,s} - \langle g_Z \rangle_s]^2 \right\}^{1/2} + \left\{ \sum_{i_s, j_s} [g_Z(\lambda_{N_{i_s}}, \lambda_{N_{j_s}}) - \langle g_Z(\lambda_{N_{i_s}}) \rangle_{N,s} - \langle g_Z(\lambda_{N_{j_s}}) \rangle_{N,s} + \langle g_Z \rangle_{N,s}]^2 \right\}^{1/2} \\
&\quad + |\langle h_Z \rangle_s| + 2 \left\{ \sum_{i_s} [\langle h_Z(\lambda_{N_{i_s}}) \rangle_{N,s} - \langle h_Z \rangle_s]^2 \right\}^{1/2} + \left\{ \sum_{i_s, j_s} [h_Z(\lambda_{N_{i_s}}, \lambda_{N_{j_s}}) - \langle h_Z(\lambda_{N_{i_s}}) \rangle_{N,s} - \langle h_Z(\lambda_{N_{j_s}}) \rangle_{N,s} \right. \\
&\quad \left. + \langle h_Z \rangle_{N,s}]^2 \right\}^{1/2} + s_L^{\nu\mu} \sum_{j_b} \sum_{l=1}^{n_G} s_L^{\nu l} B_{l N_{j_b}}^0 B_{e N_{j_b}}^0 (\langle g_Z(\lambda_{N_{j_b}}) \rangle_{N,s} + \langle h_Z(\lambda_{N_{j_b}}) \rangle_{N,s} + \{[g_Z(\lambda_{N_{i_s}}, \lambda_{N_{j_b}}) - \langle g_Z(\lambda_{N_{j_b}}) \rangle_{N,s}]^2\}^{1/2}) \\
&\quad + \{[h_Z(\lambda_{N_{i_s}}, \lambda_{N_{j_b}}) - \langle h_Z(\lambda_{N_{j_b}}) \rangle_{N,s}]^2\}^{1/2}) + s_L^{\nu e} \sum_{i_b} \sum_{l=1}^{n_G} s_L^{\nu l} B_{l N_{i_b}}^0 B_{e N_{i_b}}^0 (\langle g_Z(\lambda_{N_{i_b}}) \rangle_{N,s} + \langle h_Z(\lambda_{N_{i_b}}) \rangle_{N,s} + \{[g_Z(\lambda_{N_{i_b}}, \lambda_{N_{j_s}}) \\
&\quad - \langle g_Z(\lambda_{N_{i_b}}) \rangle_{N,s}]^2\}^{1/2} + \{[h_Z(\lambda_{N_{i_b}}, \lambda_{N_{j_s}}) - \langle h_Z(\lambda_{N_{i_b}}) \rangle_{N,s}]^2\}^{1/2}) + \sum_{i_b, j_b} \sum_{l=1}^{n_G} B_{l N_{i_b}}^0 B_{e N_{i_b}}^0 B_{l N_{j_b}}^0 B_{e N_{j_b}}^0 \{ |g_Z(\lambda_{N_{i_b}}, \lambda_{N_{j_s}})| \\
&\quad + |h_Z(\lambda_{N_{i_b}}, \lambda_{N_{j_s}})| \}, \\
|F_{box}^{\mu e d a d b}| &\leq \delta_{d_a d_b} \left(s_L^{\nu\mu} s_L^{\nu e} \left[|\langle \tilde{f}_{box} \rangle_s| + \left\{ \sum_{i_s} [\tilde{f}_{box}(\lambda_{N_{i_s}}) - \langle \tilde{f}_{box} \rangle_s]^2 \right\}^{1/2} \right] + \sum_{i_b} B_{\mu N_{i_b}}^0 B_{e N_{i_b}}^0 |\tilde{f}_{box}(\lambda_{N_{i_b}})| \right) \\
&\quad + \sum_{j=1}^{n_G} |V_{u_j d_a}| |V_{u_j d_b}| \left[s_L^{\nu\mu} s_L^{\nu e} \left(\left\{ \sum_{i_s} [f_{box}(\lambda_{N_{i_s}}, \lambda_{u_j}) - \langle f_{box}(\lambda_{u_j}) \rangle_{N,s}]^2 \right\}^{1/2} + |\langle f_{box}(\lambda_{u_j}) \rangle_{N,s}| \right) \right. \\
&\quad \left. + \sum_{i_b} B_{\mu N_{i_b}}^0 B_{e N_{i_b}}^0 |f_{box}(\lambda_{N_{i_b}}, \lambda_{u_j})| \right], \\
|F_{box}^{\mu e u u}| &\leq s_L^{\nu\mu} s_L^{\nu e} \left[|\langle \tilde{h}_{box} \rangle_s| + \left\{ \sum_{i_s} [\tilde{h}_{box}(\lambda_{N_{i_s}}) - \langle \tilde{h}_{box} \rangle_s]^2 \right\}^{1/2} \right] + \sum_{i_b} B_{\mu N_{i_b}}^0 B_{e N_{i_b}}^0 |\tilde{h}_{box}(\lambda_{N_{i_b}})| \\
&\quad + \sum_{j=1}^{n_G} |V_{u_d j}| |V_{u_d j}| \left[s_L^{\nu\mu} s_L^{\nu e} \left(\left\{ \sum_{i_s} [h_{box}(\lambda_{N_{i_s}}, \lambda_{d_j}) - \langle h_{box}(\lambda_{u_j}) \rangle_{N,s}]^2 \right\}^{1/2} + |\langle h_{box}(\lambda_{d_j}) \rangle_{N,s}| \right) \right. \\
&\quad \left. + \sum_{i_b} B_{\mu N_{i_b}}^0 B_{e N_{i_b}}^0 |h_{box}(\lambda_{N_{i_b}}, \lambda_{u_j})| \right]. \tag{B9}
\end{aligned}$$

The subscripts s and b denote heavy neutrinos satisfying Eq. (18) and Eq. (19), respectively. The $\langle \rangle$ is the average over two s heavy neutrinos and $\langle \rangle_{N,s}$ is the average over one s heavy neutrino. Expressions (B8) and (B9) are used for evaluation of UBBRs of LFV decays for any set of values of parameters. For any process the results are compared, and the smallest one is kept as a UBBR of the process.

APPENDIX C: THE CHIRAL LAGRANGIAN

The gauged chiral $U(3)_L \times U(3)_R / U(3)_V$ Lagrangian extended by hidden $U(3)_{local}$ symmetry and the mass for the pseudoscalar mesons comprises four terms,

$$\mathcal{L} = \mathcal{L}_A + a\mathcal{L}_V + \mathcal{L}_{mass} + \mathcal{L}_{kin}. \tag{C1}$$

Here only the second term is of interest or, more specifically, only the interactions of K^{0*} and \bar{K}^{0*} mesons with pseudo-scalar mesons [27],

$$\begin{aligned}
a\mathcal{L}_V = & \frac{-iga}{4} \{ K^{0*,\mu} (-\sqrt{2}\pi^+ \vec{\partial}_\mu K^- + \pi^0 \vec{\partial}_\mu \bar{K}^0 \\
& + \sqrt{3}c_P \bar{K}^0 \vec{\partial}_\mu \eta + \sqrt{3}s_P \bar{K}^0 \vec{\partial}_\mu \eta') \\
& + \bar{K}^{0*,\mu} (\sqrt{2}\pi^- \vec{\partial}_\mu K^+ - \pi^0 \vec{\partial}_\mu K^0 - \sqrt{3}c_P K^0 \vec{\partial}_\mu \eta \\
& - \sqrt{3}s_P K^0 \vec{\partial}_\mu \eta') + 2\rho^{0*,\mu} \pi^+ \vec{\partial}_\mu \pi^- \} + \dots \tag{C2}
\end{aligned}$$

The parameter a is a free parameter, equal to 2 if the vector meson dominance is satisfied, g is the coupling of (hidden-symmetry-induced) vector mesons to the chiral fields (pseu-

doscalar meson fields in the unitary gauge [30]). The $\rho^0\pi^+\pi^-$ interaction term is included because it defines experimentally known $g_{\rho\pi\pi}$ coupling ($g_{\rho\pi\pi}=ga/2$). The other vector-meson–pseudoscalar-meson couplings are fixed when $g_{\rho\pi\pi}$ is known.

Notice that the sum of $K^{0*}\pi^0\bar{K}^0$ and $\bar{K}^{0*}\pi^0K^0$ couplings is zero,

$$g_{K^{0*}\pi^0\bar{K}^0} + g_{\bar{K}^{0*}\pi^0K^0} = 0. \quad (\text{C3})$$

For that reason the $K_L \rightarrow \pi^0 \mu^+ e^-$ amplitude has a zero value. Equation (C3) remains valid even if the $U(3)_L \times U(3)_R / U(3)_V$ symmetry is broken in the way of Bando, Kugo, and Yamawaki [30].

APPENDIX D: PHASE-SPACE FUNCTIONS

The absolute squares of the LFV semileptonic hadronic amplitudes $H \rightarrow H' e^- \mu^+$ may be expressed in terms of the Mandelstam variables $t = (p_H - p_{H'})^2$ and $s_1 = (p_H - p_\mu)^2$. The corresponding decay rates read

$$\begin{aligned} \Gamma(H \rightarrow H' e^- \mu^+) &= \frac{1}{256\pi^3 m_H^3} \int_{(m_e+m_\mu)^2}^{(m_H-m_{H'})^2} dt \\ &\times \int_{s_1^-}^{s_1^+} ds_1 \langle |T(H \rightarrow H' e^- \mu^+)|^2 \rangle, \end{aligned} \quad (\text{D1})$$

where $\langle |T(H \rightarrow H' e^- \mu^+)|^2 \rangle$ is the square of the amplitude averaged over initial and summed over final leptons. The boundary s_1 values $s_1^\pm(t)$ are

$$s_1^\pm(t) = m_H^2 + m_\mu^2 + \frac{B(t)}{A(t)} \pm \frac{\sqrt{B(t)^2 - 4A(t)C(t)}}{A(t)}, \quad (\text{D2})$$

where

$$\begin{aligned} A(t) &= 4t, \quad B(t) = -2(m_H^2 - m_{H'}^2 + t)(t + m_\mu^2 - m_e^2), \\ C(t) &= m_H^2(t + m_\mu^2 - m_e^2)^2 + m_\mu^2 \lambda(m_H^2, m_{H'}^2, t), \end{aligned} \quad (\text{D3})$$

and $\lambda(x, y, z) = x^2 + y^2 + z^2 - 2xy - 2xz - 2yz$. The integration over one of the Mandelstam variables, say, s_1 , is easily performed. The remaining t integration has to be done numerically. The decay rate $\Gamma(K^+ \rightarrow \pi^+ e^- \mu^+)$ comprises t integrals A_{++} , A_{+-} , and A_{--} given by

$$\begin{aligned} A_{++} &= -4S_1^2 + 4S_1^1(-t + m_{K^+}^2 + m_{\pi^+}^2 + m_e^2 + m_\mu^2) \\ &\quad + S_1^0[t(m_e^2 + m_\mu^2) - 4m_{K^+}^2 m_{\pi^+}^2 - (m_e^2 + m_\mu^2)^2], \\ A_{+-} &= -4S_1^1(m_\mu^2 - m_e^2) \\ &\quad + S_1^0[-2t(m_\mu^2 - m_e^2) + 2(m_\mu^2 - m_e^2)(m_{K^+}^2 + m_{\pi^+}^2 \\ &\quad + m_e^2 + m_\mu^2) + (m_\mu^2 + m_e^2)(m_{K^+}^2 - m_{\pi^+}^2)], \\ A_{--} &= S_1^0[t(m_\mu^2 + m_e^2) - (m_\mu^2 - m_e^2)^2], \end{aligned} \quad (\text{D4})$$

where

$$S_1^n = \int_{s_1^-}^{s_1^+} ds_1 s_1^n. \quad (\text{D5})$$

The decay rates $\Gamma(B \rightarrow B' e^- \mu^+)$ contain t integrals A_1 , A_2 , A_3 , A_4 , and A_5 :

$$\begin{aligned} A_1 &= \frac{1}{2} S_1^2 + S_1^1 \left(\frac{1}{2} (m_B^2 + m_{B'}^2 + m_e^2 + m_\mu^2 - t) + S_1^0 [-2m_B^2 m_{B'}^2 \right. \\ &\quad \left. - 2m_e^2 m_\mu^2 - (m_B^2 + m_{B'}^2)(m_e^2 + m_\mu^2)] \right) + \frac{1}{4} \left((m_B^2 + m_{B'}^2 \right. \\ &\quad \left. + m_e^2 + m_\mu^2) t - \frac{1}{4} t^2 \right), \\ A_2 &= S_1^0 \left(\frac{1}{2} m_B m_{B'} (m_e^2 + m_\mu^2) - \frac{1}{2} m_B m_{B'} t \right), \\ A_3 &= S_1^1 t + S_1^0 \left(\frac{1}{2} (m_\mu^2 - m_e^2)(m_B^2 - m_{B'}^2) - \frac{1}{2} (m_B^2 + m_{B'}^2 \right. \\ &\quad \left. + m_e^2 + m_\mu^2) t + \frac{1}{2} t^2 \right), \\ A_4 &= S_1^1 \left(\frac{1}{2} (m_\mu^2 - m_e^2)(m_B^2 - m_{B'}^2) \right) + S_1^0 \left(\frac{1}{2} m_B (m_B^2 m_e^2 \right. \\ &\quad \left. + m_e^4 - m_{B'}^2 m_\mu^2 - m_e^2 m_\mu^2) - \frac{1}{2} m_{B'} (m_B^2 m_\mu^2 + m_\mu^4 \right. \\ &\quad \left. - m_B^2 m_e^2 - m_e^2 m_\mu^2) - \frac{1}{2} t (m_B^2 m_e^2 + m_{B'}^2 m_\mu^2) \right), \\ A_5 &= S_1^0 \left(-\frac{t^2}{8} (m_e^2 + m_\mu^2) + \frac{t}{8} [(m_e^2 + m_\mu^2)(m_B - m_{B'})^2 \right. \\ &\quad \left. + (m_\mu^2 - m_e^2)^2] - \frac{1}{8} (m_B - m_{B'})^2 (m_\mu^2 - m_e^2)^2 \right). \end{aligned} \quad (\text{D6})$$

[1] Particle Data Group, R. M. Barnett *et al.*, Phys. Rev. D **54**, 1 (1996).

[2] R. D. Peccei, *Overview of Kaon Decay Physics*, presented at International Symposium on Nuclear and Particle Physics, Meson Beams, Tokyo, Japan, 1995, UCLA-95-TEP-12, hep-ph/9504392.

[3] BNL E791 Collaboration, K. Arisaka *et al.*, Phys. Rev. Lett. **70**, 1049 (1993); T. Akagi *et al.*, Phys. Rev. D **51**, 2061 (1995).

[4] A. M. Lee *et al.*, Phys. Rev. Lett. **64**, 165 (1990); C. Campagnari *et al.*, *ibid.* **61**, 2062 (1988).

[5] A. Pich, *Rare Kaon Decays*, Invited talk at Workshop on K

- Physics, Orsay, France, 1996, FTUV-96-65, hep-ph/9610243.
- [6] P. Depommier and C. Leroy, *Rep. Prog. Phys.* **58**, 61 (1995).
- [7] J. L. Ritchie and S. G. Wojcicki, *Rev. Mod. Phys.* **65**, 1149 (1993).
- [8] J. L. Hewett, T. Takeuchi, and S. Thomas, "Indirect probes of new Physics," SLAC-PUB-7088, CERN-TH/96-56, 1996, hep-ph/9603391.
- [9] A. Pilaftsis, *Z. Phys. C* **55**, 275 (1992).
- [10] J. Bernabéu, A. Santamaria, J. Vidal, A. Mendez, and J. W. F. Valle, *Phys. Lett. B* **187**, 303 (1987); C. G. Branco, M. N. Rebelo, and J. W. F. Valle, *ibid.* **225**, 385 (1989); M. Dittmar, A. Santamaria, M.-C. Gonzales-Garcia, and J. W. F. Valle, *Nucl. Phys.* **B332**, 1 (1990).
- [11] B. McWilliams and L.-F. Li, *Nucl. Phys.* **B179**, 62 (1981); M. Sher and Y. Yuan, *Phys. Rev. D* **44**, 1461 (1991); S. T. Petcov, *Phys. Lett.* **115B**, 401 (1982).
- [12] B. Mukhopadhyaya and A. Raychaudhuri, *Phys. Rev. D* **42**, 3215 (1990); T. Kosmas, G. K. Leontaris, and J. D. Vergados, *Phys. Lett. B* **219**, 457 (1989); M. L. Levine, *Phys. Rev. D* **36**, 1329 (1987); A. Mendez and L. M. Mir, *ibid.* **40**, 251 (1989); F. Borzumati and A. Masiero, *Phys. Rev. Lett.* **57**, 961 (1986); F. Gabbiani and A. Masiero, *Nucl. Phys.* **B332**, 235 (1989).
- [13] J. Wu, S. Urano, and R. Arnowitt, *Phys. Rev. D* **47**, 4006 (1993).
- [14] R. N. Mohapatra and G. Senjanović, *Phys. Rev. D* **23**, 165 (1981); R. N. Mohapatra, *ibid.* **46**, 2990 (1992); R. N. Mohapatra, S. Nussinov, and X. Zhang, *ibid.* **49**, 2410 (1994).
- [15] Z. Gagyi-Palffy, A. Pilaftsis, and K. Schilcher, *Phys. Lett. B* **343**, 275 (1995); Z. Gagyi-Palffy, A. Pilaftsis, and K. Schilcher, "Gauge independent analysis of $K(L) \rightarrow e\mu$ in left-right models," hep-ph/9707517, 1997.
- [16] S. Dimopoulos and J. Ellis, *Nucl. Phys.* **B182**, 505 (1981); S. F. King, *ibid.* **B320**, 487 (1989).
- [17] J. C. Pati and A. Salam, *Phys. Rev. D* **10**, 275 (1974); G. L. Kane and R. Thun, *Phys. Lett.* **94B**, 513 (1980).
- [18] T. Yanagida, in *Proceedings of the Workshop on Unified Theory and Baryon Number of the Universe*, Tsukuba, Japan, 1979, edited by O. Swada and A. Sugamoto (KEK, 1979), p. 95; M. Gell-Mann, P. Ramond, and R. Slansky, *Supergravity*, Proceedings of the Workshop, Stony Brook, New York, 1979, edited by P. van Nieuwenhuizen and D. Freedman (North-Holland, Amsterdam, 1979), p. 315; R. N. Mohapatra and G. Senjanović, *Phys. Rev. Lett.* **44**, 912 (1980).
- [19] B. A. Kniehl and A. Pilaftsis, *Nucl. Phys.* **B474**, 286 (1996).
- [20] A. Ilakovac and A. Pilaftsis, *Nucl. Phys.* **B437**, 491 (1995).
- [21] E. Witten, *Nucl. Phys.* **B268**, 79 (1986).
- [22] R. N. Mohapatra and J. W. F. Valle, *Phys. Rev. D* **34**, 1642 (1986).
- [23] D. Wyler and L. Wolfenstein, *Nucl. Phys.* **B218**, 205 (1983).
- [24] I. Melo, "The phenomenology of neutral heavy leptons," Ph.D. thesis, hep-ph/9612488, 1996.
- [25] J. G. Körner, A. Pilaftsis, and K. Schilcher, *Phys. Rev. D* **47**, 1080 (1993).
- [26] A. Ilakovac, B. A. Kniehl, and A. Pilaftsis, *Phys. Rev. D* **52**, 3993 (1995).
- [27] A. Ilakovac, *Phys. Rev. D* **54**, 5653 (1996).
- [28] P. Kalyniak and L. Melo, *Phys. Rev. D* **55**, 1453 (1997).
- [29] M. S. Chanowitz, M. A. Furman, and I. Hinchliffe, *Nucl. Phys.* **B153**, 402 (1979); L. Durand, J. M. Johnson, and J. L. Lopez, *Phys. Rev. Lett.* **64**, 1215 (1990); *Phys. Rev. D* **45**, 3112 (1992). The relativistic form of partial wave amplitudes may be found in Ref. [1].
- [30] M. Bando, T. Kugo, and K. Yamawaki, *Phys. Rep.* **54**, 217 (1988); *Nucl. Phys.* **B259**, 493 (1985).
- [31] E. D. Commins and P. H. Bucksbaum, *Weak Interactions of Leptons and Quarks* (Cambridge University Press, Cambridge, England, 1983); J. F. Donoghue, E. Golowich and B. R. Holstein, *Dynamics of the Standard Model* (Cambridge University Press, Cambridge, England, 1992).
- [32] P. Herceg and T. Oka, *Phys. Rev. D* **29**, 475 (1984).
- [33] Particle Data Group, L. Montanet *et al.*, *Phys. Rev. D* **50**, 1173 (1994); Particle Data Group, K. Hikasa *et al.*, *ibid.* **45**, S1 (1992).
- [34] CDF Collaboration, F. Abe *et al.*, *Phys. Rev. Lett.* **74**, 2626 (1995); D0 Collaboration, S. Abachi *et al.*, *ibid.* **74**, 2632 (1995).
- [35] T. Appelquist and J. Carazzone, *Phys. Rev. D* **11**, 2856 (1975); G. Senjanović and A. Šokorac, *Nucl. Phys.* **B164**, 305 (1980); Y. Kazama and Y.-P. Yao, *Phys. Rev. D* **25**, 1605 (1982), and references cited therein.